Hydrol. Earth Syst. Sci., 29, 5755–5775, 2025 https://doi.org/10.5194/hess-29-5755-2025 © Author(s) 2025. This work is distributed under the Creative Commons Attribution 4.0 License.





# Reducing hydrological uncertainty in large mountainous basins: the role of isotope, snow cover, and glacier dynamics in capturing streamflow seasonality

Diego Avesani<sup>1</sup>, Yi Nan<sup>2</sup>, and Fuqiang Tian<sup>2,3</sup>

Correspondence: Yi Nan (ny1209@qq.com)

Received: 12 February 2025 – Discussion started: 17 March 2025

Revised: 31 July 2025 - Accepted: 28 August 2025 - Published: 27 October 2025

Abstract. Hydrological modeling in large mountainous catchments faces challenges owing to the complex interplay of snowmelt, glacier dynamics, and groundwater contributions, which introduce significant uncertainty in streamflow predictions. This study introduces a Bayesian multiobjective parameter estimation framework to reduce predictive streamflow uncertainty in large mountainous catchments by integrating streamflow likelihood with three auxiliary likelihoods, analyzed individually: snow cover area (SCA), glacier mass balance (GMB), and isotopic composition (I). The well-established generalized likelihood uncertainty estimation (GLUE) method is employed to investigate trade-offs among these likelihoods, providing a detailed assessment of their distinct and combined contributions to hydrological model performance across various flow regimes. The semi-distributed tracer-aided Tsinghua representative elementary watershed-tracer (THREW-T) hydrological model applied in this work captures both rapid surface dynamics and slow-response subsurface processes, offering a comprehensive representation of streamflow variability.

Results indicate that isotopic likelihood plays a critical role in reducing low-flow uncertainty by effectively constraining subsurface flow and groundwater—surface water interactions, particularly during winter and early spring when these processes dominate. Conversely, while SCA and GMB likelihoods demonstrate some effectiveness in capturing rapid processes such as snowmelt and glacier melt, their influence is most pronounced during the melting season, with limited effect on reducing overall streamflow un-

certainty. This seasonality is reflected in sharpness (SH) values, which measure how much uncertainty is reduced, with isotopic likelihood achieving the highest peak of 0.34 in late winter, whereas SCA and GMB reach maximum SH values of 0.19 and 0.16, respectively, during the melting season. Pareto plots further reveal the synergies and trade-offs associated with each likelihood, underscoring the importance of adopting a multi-objective calibration approach that accounts for seasonal variations in hydrological processes. In addition, the results highlight the critical role of seasonality in shaping the effectiveness of auxiliary likelihoods, emphasizing their potential to improve predictive accuracy and reduce uncertainty in hydrological models.

# 1 Introduction

Accurate hydrological modeling in large mountainous catchments remains particularly challenging owing to the inherent complexity of these systems (Gupta et al., 2008). The interplay of multiple water sources, such as snowmelt, glacier dynamics, and groundwater, combined with substantial spatiotemporal variability in streamflow generation, often results in equifinality and significant uncertainty in predictions (e.g., Asong et al., 2020; Shuai et al., 2022; Dalla Torre et al., 2024). These complexities call for advanced modeling approaches capable of improving our understanding of streamflow variability and supporting effective water resource management (Panchanathan et al., 2024).

<sup>&</sup>lt;sup>1</sup>Department of Civil, Environmental and Mechanical Engineering, University of Trento, 38123 Trento, Italy

<sup>&</sup>lt;sup>2</sup>State Key Laboratory of Hydroscience and Engineering, Tsinghua University, Beijing 100084, China

<sup>&</sup>lt;sup>3</sup>Department of Hydraulic Engineering, Tsinghua University, Beijing 100084, China

Recent advancements in hydrological modeling have addressed these demands by focusing on the integration of auxiliary variables, such as snow cover area (SCA), glacier mass balance (GMB), and environmental tracers (e.g., stable oxygen isotopes,  $\delta^{18}$ O), to improve model calibration and reduce parameter uncertainty (Di Marco et al., 2021; Nan et al., 2021b; Mohammadi et al., 2023). These variables provide critical insights into cryospheric and subsurface processes, enabling models to better capture hydrological responses that drive streamflow variability during periods of low flow (Panchanathan et al., 2024). Incorporating such data improves the representation of specific model components and guides the evaluation of the model, ultimately enhancing reliability and reducing equifinality (Birkel et al., 2014; Tetzlaff et al., 2014). Tracer-aided modeling has proven particularly effective in disentangling hydrological processes and identifying critical contributions from snowmelt and groundwater under varying conditions (Nan et al., 2021b). Bayesian approaches have also been applied to explicitly address equifinality and uncertainty in hydrological modeling in various mountain basins (e.g., Yang et al., 2007; Andraos, 2024).

Nonetheless, several challenges remain. Few studies have systematically compared the relative effectiveness of auxiliary datasets - such as SCA, GMB, and isotopic tracers in reducing model uncertainty and equifinality across different flow regimes (Finger et al., 2011; Xu et al., 2012; Nan and Tian, 2024). While some studies have explored the role of individual datasets, such as isotopic tracers (Nan and Tian, 2024) or GMB (Finger et al., 2011), a unified comparison of their respective contributions within a single modeling framework remains absent. This is particularly true for low-flow conditions, which are often dominated by slowresponse processes such as groundwater contributions and subsurface flow dynamics (Betterle and Bellin, 2024). Moreover, the potential for these datasets to improve the representation of hydrological processes under varying seasonal conditions remains largely unexplored. Similarly, while previous work has explored the contributions of runoff components (CRC) to total streamflow (e.g., subsurface flow, rainfall runoff, snowmelt, and glacier melt) (Stahl et al., 2008), a comprehensive understanding of how these components interact to influence streamflow dynamics under different conditions remains insufficiently constrained by multi-source datasets. Current Bayesian frameworks, while powerful, often fail to fully leverage the complementary strengths of auxiliary datasets, particularly in large mountainous catchments where complex cryospheric and subsurface interactions drive streamflow dynamics (Zhang et al., 2018; Chang et al., 2024).

This study addresses these gaps by systematically evaluating the role of SCA, GMB, and isotopic tracers in reducing model uncertainty and equifinality within a fully Bayesian framework. Focusing on the Yarlung Tsangpo River (YTR) basin – a large mountainous catchment where streamflow variability arises from snowmelt, glacier dynamics, and

groundwater contributions – we investigate how these auxiliary datasets can complement each other in constraining hydrological models across different flow regimes. Special emphasis is placed on low-flow periods, during which isotopic data provide particularly strong constraints on subsurface flow and groundwater—surface water interactions (Rodgers et al., 2005). By adopting a multi-source calibration approach, we explore trade-offs in model performance and quantify how each dataset influences the contributions of snowmelt, glacier melt, rainfall runoff, and subsurface flow. By shedding light on streamflow generation processes, particularly during low-flow periods, these findings may offer a first step toward more integrated and nuanced water management strategies in complex mountainous regions facing increasing drought risk (Wu et al., 2023).

To address these objectives, the paper is organized as follows: the adopted tracer-aided hydrological model, the study area, and the Bayesian framework are described in Sect. 2. In Sect. 3, we present the results, including parameter distributions, uncertainty analysis, and flow regime-specific improvements. In Sect. 4, we discuss the implications of the findings, while in Sect. 5, we provide concluding remarks and future research directions.

#### 2 Materials and methods

#### 2.1 Study area and data

The YTR basin was selected as the focus area of this study (Fig. 2); the basin is the upstream part of the Brahamaputra River basin, located on the southern Tibetan Plateau (TP). The YTR basin, as one of the longest rivers originating from the TP, extends in the range of 27–32° N and 82–97° E with an elevation extent of 2900-6900 m above sea level. The outlet hydrological station of the YTR basin is the Nuxia station, with a drainage area of approximately  $2 \times 10^5$  km<sup>2</sup>. There are four hydrological stations along the mainstream of YTR: Nuxia, Yangcun, Nugesha, and Lazi, from downstream to upstream (Table 1). During 1990–2015, the mean annual precipitation in the YTR basin was approximately 490 mm, which was dominated by the South Asian monsoon in the Indian Ocean hydrosphere-atmosphere system resulting an obvious wet season during June to September. The mean annual temperature is -1.5 °C, leading to widely distributed snow and glacier, covering approximately 16.3 % and 1.5 %, respectively, of the basin.

Datasets of meteorological input, topography, underlying surface, streamflow, and isotope were collected to establish the model. The 30 m resolution digital elevation model (DEM) was downloaded from the Geospatial Data Cloud (https://www.gscloud.cn, last access: 1 January 2019) for simulation unit dividing. Daily precipitation and temperature data were extracted from the 0.1° China Meteorological Forcing Dataset (Yang and He, 2019), which was pro-

3691

4541

4715

4889

Station	Coordinate	Elevation (m)	Streamflow	Isotope				
			Period	Period (in 2005)	Precipitation		Stream water	
					number of	δ <sup>18</sup> O	number of	$\delta^{18}O$
					samples	$(\%_{o})$	samples	(%o)

14 Mar-23 Oct

14 May-22 Oct

17 Mar-5 Oct

6 Jun-22 Sep

2001-2015

2001-2010

2001-2010

**Table 1.** Data and sample information at four hydrological stations adopted.

94.65° E, 29.47° N

91.82° E, 29.27° N

89.71° E, 29.32° N

87.58° E, 29.12° N

Nuxia

Yangcun

Nugesha

Lazi

duced by merging multiple satellite datasets with the national meteorological station data. The daily potential evapotranspiration were obtained from the 1.0° reanalysis dataset ERA5 Land (Muñoz-Sabater et al., 2021). For the underlying conditions, the MODIS leaf area index (LAI) product MOD15A2H (Myneni et al., 2015) and the normalized difference vegetation index (NDVI) product MOD13A3 (Didan, 2015) were used to represent the vegetation conditions and determine the ratio of vegetation covered area, and the Harmonized World Soil Database (He, 2019) was used to estimate the soil property parameters not obtained by model calibration (including saturated hydraulic conductivity, soil porosity, soil pore distribution index, field capacity, and air entry value). For the cryospheric elements, the second glacier inventory dataset of China (Liu, 2012) was adopted to determine the boundary of regions where glacier simulation should be performed. The daily TP snow cover extent (TP-SCE) product (Chen et al., 2018) during 2001-2015 and the 0.5° yearly glacier elevation change dataset developed by Hugonnet et al. (2021) during 2001-2010 were used to validate the simulated SCA and GMB. Daily streamflow observation data at the Nuxia, Yangcun, and Nugesha stations were collected to evaluate the performance of the hydrological simulations. However, owing to Chinese national regulations, streamflow data for the YTR - a transboundary river system - are considered sensitive and classified as confidential. As such, these data cannot be publicly disclosed or shared in this publication. This restriction reflects broader geopolitical concerns, as highlighted by Lin et al. (2023), who emphasize the particular sensitivity of hydrological data in transboundary basins and regions subject to resource and geopolitical tensions. Considering the availability period of the supporting datasets, the simulation period was set from 1 January 2001 to 31 December 2015, aligned with the time span of the meteorological and vegetation input data.

Grab samples of stream and precipitation water were collected in 2005 at four stations to analyze the isotope composition ( $\delta^{18}$ O) to validate the tracer simulation (Table 1). The outputs of the Scripps Global Spectral Model with an isotope incorporated (isoGSM, Yoshimura et al., 2008) with 1.875° resolution were extracted to represent the spatiotem-

poral variation of the isotope composition in precipitation. Our previous evaluation on isoGSM (Nan et al., 2021a) indicated that it can effectively capture the seasonal variation in precipitation  $\delta^{18}$ O, but exhibited a systematic overestimation bias in the study region and performed relatively poorly in accurately capturing the isotope signature of specific events (Figs. S1 and S2 in the Supplement). The bias corrected isoGSM product produced by Nan et al. (2022) was adopted as the input data, in which the bias of isoGSM was adjusted based on a linear regression with altitude. Rainfall and snowfall were assumed to have the same isotope composition as the precipitation  $\delta^{18}$ O in isoGSM. The glacier meltwater  $\delta^{18}$ O is calculated using the offset-parameter method, in which the glacier meltwater  $\delta^{18}$ O is assumed to be temporally constant and 5% lower than the weighted average of local precipitation  $\delta^{18}$ O. The value of the offset parameter was estimated from the data collected by Boral and Sen (2020).

-10.33

-13.14

-14.29

-17.41

86

59

45

42

34

30

25

22

-15.74

-16.57

-17.84

-16.52

# 2.2 The tracer-aided hydrological model

A semi-distributed tracer-aided cryospheric-hydrological model, Tsinghua representative elementary watershed-tracer aided version (THREW-T) developed by Tian et al. (2006) and Nan et al. (2021b) was adopted to simulate the hydrological, cryospheric and isotopic processes in the YTR basin (Fig. 1). The THREW-T model uses the representative watershed method (REW) for spatial discretization, which divides the whole catchment into REWs based on DEM data. Two vertical layers including eight subzones (i.e., surface layer including vegetation zone, bare soil, sub-stream network zone, snow-covered zone, glacier-covered zone, and main channel reach zone; subsurface layer including unsaturated zone and saturated zone) are defined for each REW-based on the underlying surface type. The YTR basin was divided into 297 REWs with average area of 694 km<sup>2</sup> in this study. The areal averages of the gridded datasets were calculated for each REW, which were used as the input for simulation. More detailed descriptions of the REW method can be found in Reggiani et al. (1999) and Tian et al. (2006).

The cryospheric module was incorporated into the model to simulate the evolutions of snowpack and glacier. The total

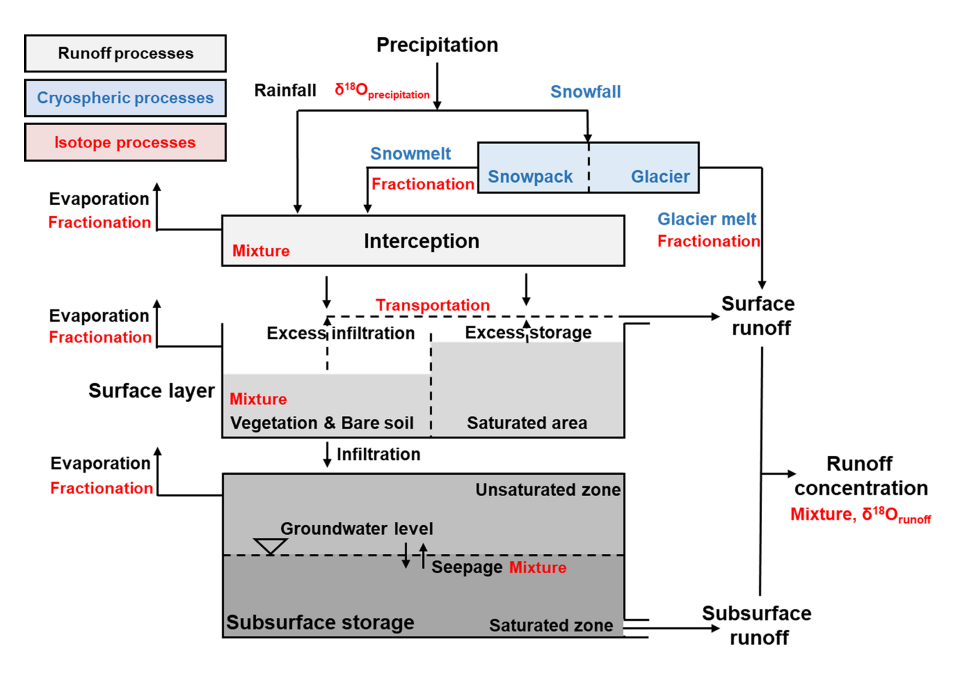
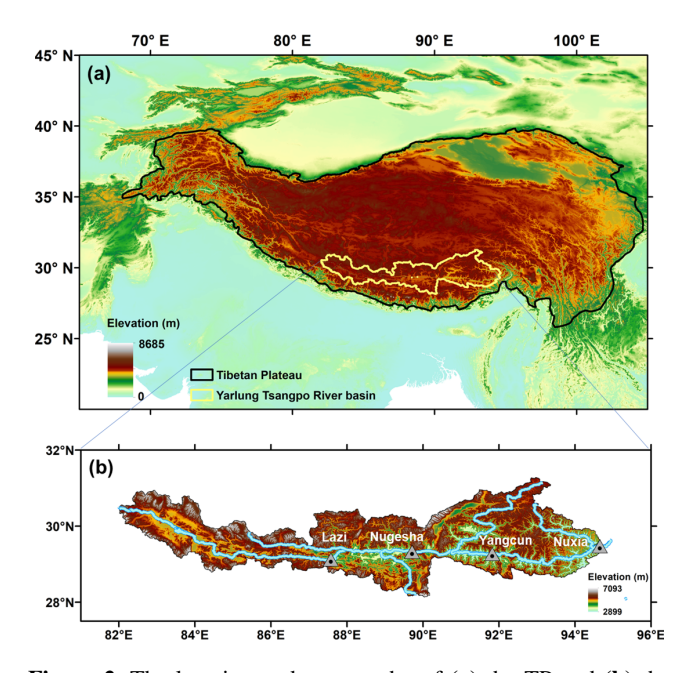


Figure 1. Schematic representation of the THREW-T model.



**Figure 2.** The location and topography of **(a)** the TP and **(b)** the YTR basin.

precipitation was partitioned into liquid (rainfall) and solid precipitation (snowfall), according to a temperature threshold set as 0 °C. For the simulation of snowpack, the snow water equivalent of each REW was updated based on the snowfall and the snowmelt, which was calculated using the degree-day factor method. The SCA was determined by the snow cover depletion curve (Fassnacht et al., 2016) and then compared with the satellite observation data. The snow sub-

limation was not simulated in the model, because previous studies estimated that the sublimation losses in the study region only accounted for 2 %–3 % of the annual snowfall, as the results of the wet climate condition (Khanal et al., 2021; Sun et al., 2024; Lutz et al., 2016). For the simulation of glacier, each REW was further divided into several elevation bands with an interval of 200 m, to represent the variation in temperature and precipitation along the altitudinal profile. The glacier within the intersection of each REW and elevation band was regarded as the representative unit for glacier simulation. The processes related to glacier evolution in the model included the snow accumulation and snowmelt over glaciers, the turnover of snow to ice, and the ice melt. The ice melt was also calculated using the temperature index method but with a different degree-day factor from snowmelt. The volume of the glacier was updated based on the mass balance equation and was transferred to the glacier cover area based on a scale equation (Grinsted, 2013). The glacier melt was assumed to generate streamflow directly through the surface pathway, considering the low permeability of glacier surface. The output of the glacier simulation included the glacier mass balance (GMB) and the glacier cover area, and the simulated GMB were compared with the measurement data. More details of the cryospheric module can be found in Nan et al. (2021b) and Cui et al. (2023).

The tracer module was incorporated into the model to simulate the isotope composition in multiple water bodies, which characterized the isotopic variations during water mixture and phase change processes. The isotope fractionation during water evaporation and snowmelt processes was simulated by the Rayleigh equation (Hindshaw et al., 2011). The isotope compositions in each simulation unit were calculated based

on the complete mixing assumption, meaning that the tracer concentration homogeneity within a unit was achieved during a simulation time step (Nan et al., 2023). Forced by the precipitation isotope input, the model can simulate the isotope composition of all the water bodies, including river water, groundwater, and snowpack, and the simulated isotope composition of river water was compared with the observation data. More details of the tracer module are provided in Nan et al. (2021b).

The CRC were analyzed to better understand the influence of multiple datasets on hydrological simulations. Two definitions are commonly used to quantify CRC (He et al., 2021). One is based on water sources, describing where the water originates; under this definition, the three components are rainfall, snowmelt, and glacier melt. The other is based on the runoff generation pathway, describing how water produces runoff; here, the two components are surface and subsurface runoff. The THREW-T model quantified the runoff components based on the definition that combines water sources and runoff generation pathways. Specifically, the runoff was first divided into surface runoff and subsurface runoff based on the runoff generation pathway. The surface runoff was further divided into three components induced by different water sources: rainfall, snowmelt, and glacier melt. Consequently, the total runoff was divided into four components: subsurface runoff, rainfall surface runoff, snowmelt surface runoff, and glacier melt surface runoff. For the sake of completeness, Table 2 reports the list of the calibration parameters of the hydrological model adopted, with their units and range of variation.

# 2.3 Multi-objective parameter estimation

The uncertainty estimation of model parameters was performed using the generalized likelihood uncertainty estimation (GLUE) methodology (Beven, 2006). GLUE employs Monte Carlo simulations to generate a large ensemble of model realizations, where each realization corresponds to a specific parameter set associated with a likelihood measure. Unlike traditional optimization methods that focus on identifying a single *best* parameter set, GLUE emphasizes equifinality by retaining an ensemble of acceptable parameterizations (Efstratiadis and Koutsoyiannis, 2010; Brazier et al., 2000), thus acknowledging that multiple parameter sets can produce similarly good simulations, which is particularly important when modeling complex hydrological systems where uncertainties in processes and inputs can lead to varied but equally plausible outcomes (Di Marco et al., 2021).

The selection of likelihood measures and thresholds to distinguish behavioral from non-behavioral simulations is inherently subjective and problem-dependent (Blasone et al., 2008; Jin et al., 2010). In this study, the parameter space was sampled using Latin hypercube sampling (McKay et al., 1979), assuming a uniform distribution for all parameters listed in Table 1. In the absence of prior information,

all parameter sets were initially considered equally probable, ensuring non-informative priors (e.g., Gan et al., 2018; Teweldebrhan et al., 2018). The effect of this uniformity assumption on posterior results was evaluated through sensitivity analyses.

A total of 25 000 parameter sets were generated and evaluated using a likelihood measure to quantify model performance. Behavioral simulations were identified based on a predefined threshold, the value of which is provided in the results section. Non-behavioral simulations were assigned a likelihood of zero, while the likelihood values of retained simulations were rescaled to sum to one, forming a posterior probability density function for the model parameters.

Predictive uncertainty of outputs, such as streamflow, was assessed by ranking behavioral simulations according to their rescaled likelihoods. The empirical cumulative distribution, weighted by these likelihoods, was used to define uncertainty bounds by excluding the lower and upper 5th percentiles (Teweldebrhan et al., 2018; Franks et al., 1998).

The Nash–Sutcliffe efficiency (NSE) index (Nash and Sutcliffe, 1970) was selected as the likelihood measure for streamflow, SCA, and I (Lamontagne and Barber, 2020; Araya et al., 2023), while the volumetric deviation efficiency (VE) (He et al., 2018) was adopted for GMB. These two metrics were chosen to reflect both dynamic performance and cumulative accuracy across key hydrological variables.

The NSE was used as the likelihood measure for streamflow, SCA, and I. Its formulation is provided for completeness:

$$NSE_X = 1 - \frac{\sum_{t=1}^{N} (X_{sim}(t) - X_{obs}(t))^2}{\sum_{t=1}^{N} (X_{obs}(t) - X_{obs,mean})^2},$$
 (1)

where X represents the variable of interest,  $X_{\text{sim}}(t)$  and  $X_{\text{obs}}(t)$  are the simulated and observed values at time step t,  $X_{\text{obs,mean}}$  is the mean of the observed values, and N is the number of time steps.

For GMB, the VE was deemed more appropriate as it directly evaluates the accuracy of the simulated mean relative to the observed mean, aligning better with the cumulative nature of GMB:

$$VE_{GMB} = 1 - \frac{GMB_{mean,sim} - GMB_{mean,obs}}{GMB_{mean,obs}},$$
 (2)

where GMB<sub>mean,sim</sub> and GMB<sub>mean,obs</sub> are the simulated and observed mean GMBs, respectively.

The multi-objective parameter estimation followed an informal Bayesian framework. The streamflow likelihood,  $LH(Q|p_i)$ , was first used to constrain the model parameters, forming the prior likelihood distribution. Auxiliary variables (X) were then incorporated to produce a posterior likelihood distribution (cLH), defined as

$$cLH(p_i|Q,X) = \frac{1}{C} \cdot LH(Q|p_i) \cdot LH(X|p_i), \tag{3}$$

Symbol	Range	Units	Description
nt	0-0.2	_	Manning roughness coefficient for hillslope
WM	0-10	m	Tension water storage capacity used to calculate the saturation area
B	0-1	_	Shape coefficient used to calculate the saturation area
Gatr	0-10	_	Coefficient representing spatial heterogeneity of exchange term between t-zone and r-zone
KKA	0-6	_	Exponential coefficient to calculate the subsurface runoff outflow rate
KKD	0-0.5	_	Linear coefficient to calculate the subsurface runoff outflow rate
$DDF_S$	0-10	$\mathrm{mm}^{\circ}\mathrm{C}^{-1}\mathrm{d}^{-1}$	Degree-day factor for snowmelt
$DDF_{G}$	0-10	${\rm mm}{}^{\circ}{\rm C}^{-1}{\rm d}^{-1}$	Degree-day factor for glacier melt
LL	0-1	_	Coefficient to transfer snow water equivalent to SCA using snow depletion curve
$T_0$	-5-5	°C	Temperature threshold above which snow and glacier melting occurs
α	0-1	_	Coefficient in the Muskingum method for runoff concentration calculation
β	0-1	_	The proportion to the $\alpha$ coefficient in the Muskingum method for runoff concentration

**Table 2.** Parameter table with descriptions, ranges, and units.

where  $p_i$  represents a parameter set,  $LH(Q|p_i)$  and  $LH(X|p_i)$  are the likelihoods for streamflow and auxiliary variables, respectively, and C is a normalization constant ensuring

$$\int cLH(p_i|Q,X)dp_i = 1.$$
(4)

In the absence of explicit guidelines for auxiliary datasets, except for streamflow, thresholds of NSE > 0 and VE > 0, commonly used as minimal performance criteria, were systematically applied to all target variables, including streamflow (Q), SCA, GMB, and I. The use of NSE > 0 for streamflow ensures consistency across all metrics, even though stricter thresholds are typically recommended to ensure the reliability of streamflow simulations (Moriasi et al., 2007). Furthermore, following Di Marco et al. (2021); Ma et al. (2024), the 75th percentile was chosen as the cutoff for both the prior and posterior distributions to select parameter sets, ensuring a consistent and robust identification of the most likely parameters while balancing model accuracy and diversity.

# 2.4 Metrics for quantifying uncertainty

To assess the added value of multi-objective model conditioning compared to single-objective approaches based solely on streamflow observations, we utilized two uncertainty metrics: the first, known as the containing ratio (CR), evaluates the ability of the simulated prediction intervals to capture the observed values and reads as follows (e.g., Teweldebrhan et al., 2018; Jin et al., 2010):

$$CR = \frac{1}{N} \sum_{t=1}^{N} \Gamma(Q_{\text{obs}}(t); Q_{\text{sim},0.05}(t), Q_{\text{sim},0.95}(t)),$$
 (5)

where  $Q_{\text{sim},0.05}(t)$  and  $Q_{\text{sim},0.95}(t)$  indicate the lower and upper bounds of the simulated 90% streamflow prediction

interval, respectively, while  $\Gamma$  returns a value of 1 if the observation falls within the prediction interval and 0 otherwise. A higher CR value indicates that the prediction intervals are better at capturing observed values, reflecting improved reliability of the model outputs. Conversely, a lower CR suggests that the prediction intervals fail to encompass the observed data as effectively, indicating potential deficiencies in the model's calibration or input data.

The second metric, SH, is a measure that quantifies the reduction in prediction uncertainty achieved through the integration of additional information and reads as follows:

$$SH = 1 - \frac{cLH(p_i \mid Q, X)}{LH(Q \mid p_i)}.$$
 (6)

A higher SH value signifies that the prediction intervals are narrower, implying reduced uncertainty in the model's predictions and a more precise representation of the streamflow dynamics. On the other hand, a lower SH value suggests broader prediction intervals, indicative of higher uncertainty or less precise modeling.

Note that in an ideal scenario, a perfectly constrained model would achieve CR and SH values close to 1. In practice, this would imply that the prediction intervals consistently capture observed values (CR=1) and that the model uncertainty diminishes to the point where the simulated output closely aligns with the observations, indicating that there is no uncertainty in the predictions.

## 3 Results

#### 3.1 Behavioral simulations

For each run of the overall Monte Carlo ensemble, we computed likelihood values for streamflow (NSE $_Q$ ) and for the additional performance metrics: SCA likelihood (NSE $_{SCA}$ ), GMB likelihood (VE $_{GMB}$ ), and isotope likelihood (NSE $_{I}$ ).

The bi-objective relationships between NSE<sub>O</sub> and each of these metrics are illustrated in Fig. 3, where each panel shows the distribution of the full ensemble of simulations. Specifically, the red markers indicate simulations on the Pareto front, defined as the subset of ensemble members that are not dominated with respect to the two metrics shown. In other words, a simulation is considered non-dominated (i.e., Pareto-optimal) if no other simulation in the ensemble performs at least as well in both objectives and strictly better in at least one (e.g., Yapo et al., 1998; Efstratiadis and Koutsoyiannis, 2010). These points thus represent optimal tradeoffs between the two objectives, as improving one necessarily implies a deterioration in the other. The Pareto front was computed over the full ensemble and independently of any behavioral classification, so red markers should not be interpreted as behavioral simulations. The blue lines in each panel indicate the thresholds used to define behavioral solutions and are included solely for visual reference. The relatively small number of Pareto-optimal simulations reflects the selective nature of such trade-offs, as most parameterizations are dominated in at least one objective. This is consistent with findings by Di Marco et al. (2021), who showed that Pareto-optimal solutions typically represent only a small subset of behavioral ones. The remaining gray points correspond to dominated simulations and delineate the broader trade-off landscape, offering insight into the variability of model performance across the ensemble.

The SCA likelihood (NSE<sub>SCA</sub>) exhibits a strong positive relationship with streamflow likelihood (NSE $_{O}$ ). As shown in Fig. 3a, the Pareto front points (red markers) are concentrated in the upper-right quadrant of the plot, indicating that high streamflow likelihood values can coexist with high NSE<sub>SCA</sub> values. This suggests strong compatibility between these two objectives, meaning that improving streamflow performance does not inherently result in a reduction in NSE<sub>SCA</sub>. The dominated solutions (gray points) show a wider spread across the plot, including regions where both NSE<sub>O</sub> and NSE<sub>SCA</sub> values are low. This indicates variability in model performance when considering different parameter sets. The clustering of Pareto-optimal solutions in the highlikelihood region reflects the shared role of snow processes in regulating both streamflow and snow cover dynamics suggest that it is possible to improve NSE<sub>SCA</sub> without significant trade-offs when calibrating the model to optimize streamflow performance.

The GMB likelihood (VE<sub>GMB</sub>) shows a slightly different behavior, as illustrated in Fig. 3b. Although high streamflow likelihood values are still associated with moderate to high VE<sub>GMB</sub> values on the Pareto front, the vertical spread of the red markers is more pronounced. This indicates a weaker synergy between these two metrics compared to NSE<sub>SCA</sub>. While some Pareto-optimal solutions achieve high likelihoods for both NSE $_Q$  and VE<sub>GMB</sub>, others show intermediate VE<sub>GMB</sub> values despite high NSE $_Q$  performance. This pattern suggests the presence of moderate trade-offs, where ac-

curately capturing glacial mass dynamics might be compromised to achieve better streamflow performance.

The isotope likelihood (NSE<sub>I</sub>) exhibits the most significant trade-offs among the three metrics, as illustrated in Fig. 3c. The Pareto front (red markers) is notably dispersed, with even the highest-performing solutions for NSE $_Q$  rarely exceeding an NSE<sub>I</sub> value of 0.4. This indicates a high degree of independence and conflict between these two metrics. The complexity of this relationship is further emphasized by the dominated solutions (gray points), where many configurations achieve high NSE $_Q$  values but fail to yield satisfactory NSE<sub>I</sub> values.

# 3.2 Prior and posterior parameter distributions

Figure 4 shows the prior (black lines) and posterior parameter distributions, conditioned on the likelihoods of SCA (SCA, orange dashed lines), GMB (GMB, light blue dash-dotted lines), and isotope concentrations (I, green dotted lines). All distributions are derived from the Monte Carlo ensemble, but only simulations with an NSE for streamflow (NSE<sub>O</sub> > 0) are retained. This threshold ensures that simulations outperform the climatological mean, thereby meeting a minimum criterion for behavioral plausibility. These behaviorally plausible simulations define the prior distribution, which is then formally updated within a Bayesian framework using the likelihoods associated with the additional observational datasets (i.e., SCA, GMB, and I). Visual inspection of the posterior distributions indicates that, in general, each dataset provides meaningful information to constrain parameters related to the physical processes it represents.

For example, the parameters DDF<sub>S</sub> and LL (Fig. 4g and i), which control SCA transfer and snowmelt processes, show a stronger response when conditioned on the likelihood of SCA, highlighting their direct influence on snow dynamics. While DDFs regulates the magnitude of snowmelt, LL primarily affects the spatial extent and persistence of snow cover. As such, its influence is more pronounced in shaping the spatial and temporal patterns of snow accumulation and melt, rather than the total amount of snowmelt contributing to runoff. This explains why the posterior of LL is well constrained under SCA conditioning, but does not manifest as clearly in metrics focused on water yield, such as snowmelt fraction. Similarly, the parameter DDF<sub>G</sub> (Fig. 4h), which governs glacier melt processes, exhibits tighter posterior constraints when conditioned on the GMB likelihood, reflecting its strong connection to ice melt dynamics. Interestingly, the parameter DDF<sub>S</sub> shows a contrasting response under the GMB likelihood, with the posterior distribution shifting in the opposite direction compared to the SCA posterior distribution.

A similar observation can be made for the isotopic likelihood, which effectively constrains parameters related to subsurface flow and runoff partitioning. For example, the parameter KKA (Fig. 4e), which defines the subsurface runoff out-

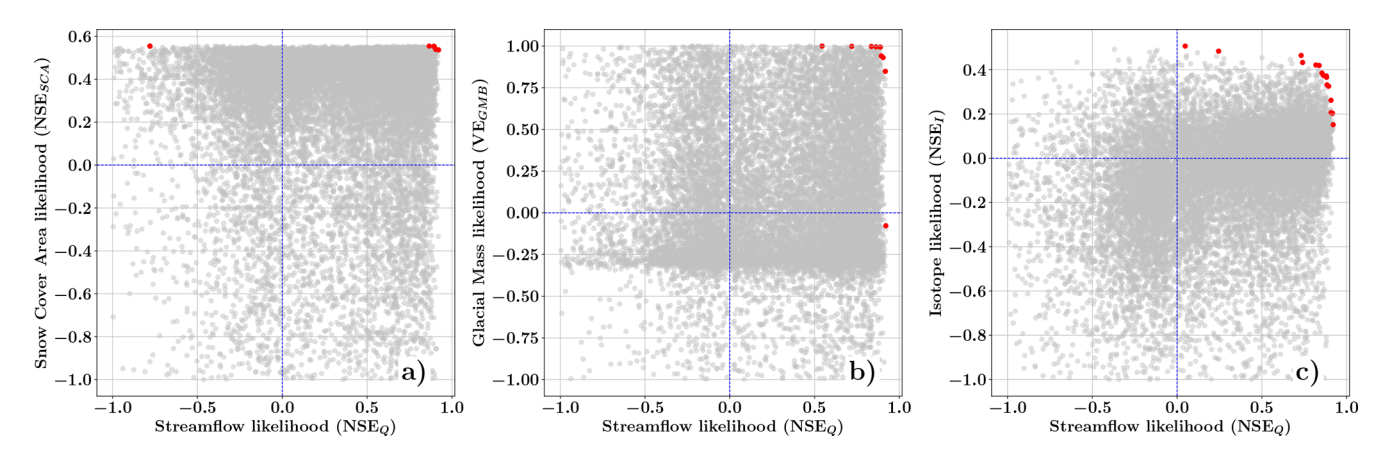


**Figure 3.** Pareto fronts (red markers) of streamflow likelihood (NSE $_Q$ ) and likelihood metrics for (a) SCA likelihood (NSE $_{SCA}$ ), (b) GMB likelihood (VE $_{GMB}$ ), and (c) Isotope likelihood (NSE $_I$ ). The thin blue lines represent the performance thresholds defined for the multi-objective behavioral selection: NSE $_Q$  = 0, NSE $_{SCA}$  = 0, NSE $_I$  = 0, and NSE $_{GMB}$  = 0. The dominated solutions are shown as gray points.

flow rate, shows noticeable convergence when conditioned on isotope data. Although both KKA and KKD influence subsurface runoff outflow, only KKA shows a marked posterior convergence. This is probably due to its exponential formulation, which increases its sensitivity to the calibration targets, whereas KKD, as a linear coefficient, exerts a more gradual influence that is harder to isolate and constrain. Other parameters, such as the tension water storage capacity WM (Fig. 4b) and the shape coefficient B (Fig. 4c), which influence the calculation of the saturation area, also exhibit tighter posterior distributions, underscoring the capacity of isotope data to inform processes related to water storage and release in the subsurface. Furthermore, the runoff concentration coefficients  $\alpha$  and  $\beta$  (Fig. 4k and 1) are better estimated with the inclusion of isotopic data with respect to the likelihoods of SCA and GMB.

An interesting case is the temperature threshold parameter  $T_0$  (Fig. 4j), which defines the threshold above which snow and glacier melting occur. The SCA likelihood has the strongest influence on the posterior distribution of  $T_0$ . However, both the GMB and the isotopic likelihoods can narrow the posterior distribution of  $T_0$ , albeit to a lesser extent, indicating that the GMB and the isotopic data provide complementary constraints on this parameter.

In contrast, the posterior distribution of the parameter Gatr shows minimal variation compared to the previous (Fig. 4d), aligning with expectations, as Gatr reflects spatial heterogeneity, which reduces its sensitivity to individual physical processes. Note that for the parameter nt, not only does none of the data sets (SCA, GMB, or I) significantly constrain the posterior distribution compared to the prior, but the isotopic likelihood appears counterproductive in this case, as it increases the uncertainty by broadening the posterior distribution and reducing its peak.

#### 3.3 Streamflow simulation uncertainty range

The prior and posterior likelihood distributions, as described in Sect. 2, were used to estimate the 5th-95th percentile prediction uncertainty ranges for daily streamflow simulations. Figure 5 illustrates these predictive uncertainty ranges in comparison to observed streamflow data recorded at the Nuxia gauging station. Owing to dissemination restrictions imposed by the data provider, streamflow values are presented in normalized form throughout the figure. Specifically, a linear normalization is applied to the time series panels to enable relative comparison of flow magnitude over time, while a logarithmic normalization is used in the flow duration curves (FDCs), as is standard in FDC representation, to facilitate comparison across the full range of discharges. The prior uncertainty, represented by dark gray bands, corresponds to the hydrological model conditioned solely on observed streamflow. By contrast, the posterior uncertainty ranges, shown as lighter bands, result from the integration of additional datasets: SCA, GMB, and isotopic data. Overall, the uncertainty bands are effective in capturing the observed streamflow values. This is confirmed by the containing ratio (CR) metric, which indicates that the prior distribution encloses approximately 96 % of the observations (CR = 0.959). Posterior distributions derived from isotopic likelihoods show a slightly lower coverage (CR = 0.921), while those incorporating SCA and GMB yield CR values of 0.947 and 0.960, respectively. These results suggest that, although SCA and GMB maintain similar levels of coverage compared to the prior, they do not lead to a substantial reduction in predictive reliability. Conversely, the posterior conditioned on isotopic data demonstrates a modest decrease in coverage, indicating a more selective constraint on the model's predictive range.

Inspection of Fig. 5 indicates no reductions in uncertainty bands for higher streamflow values across all scenarios. On

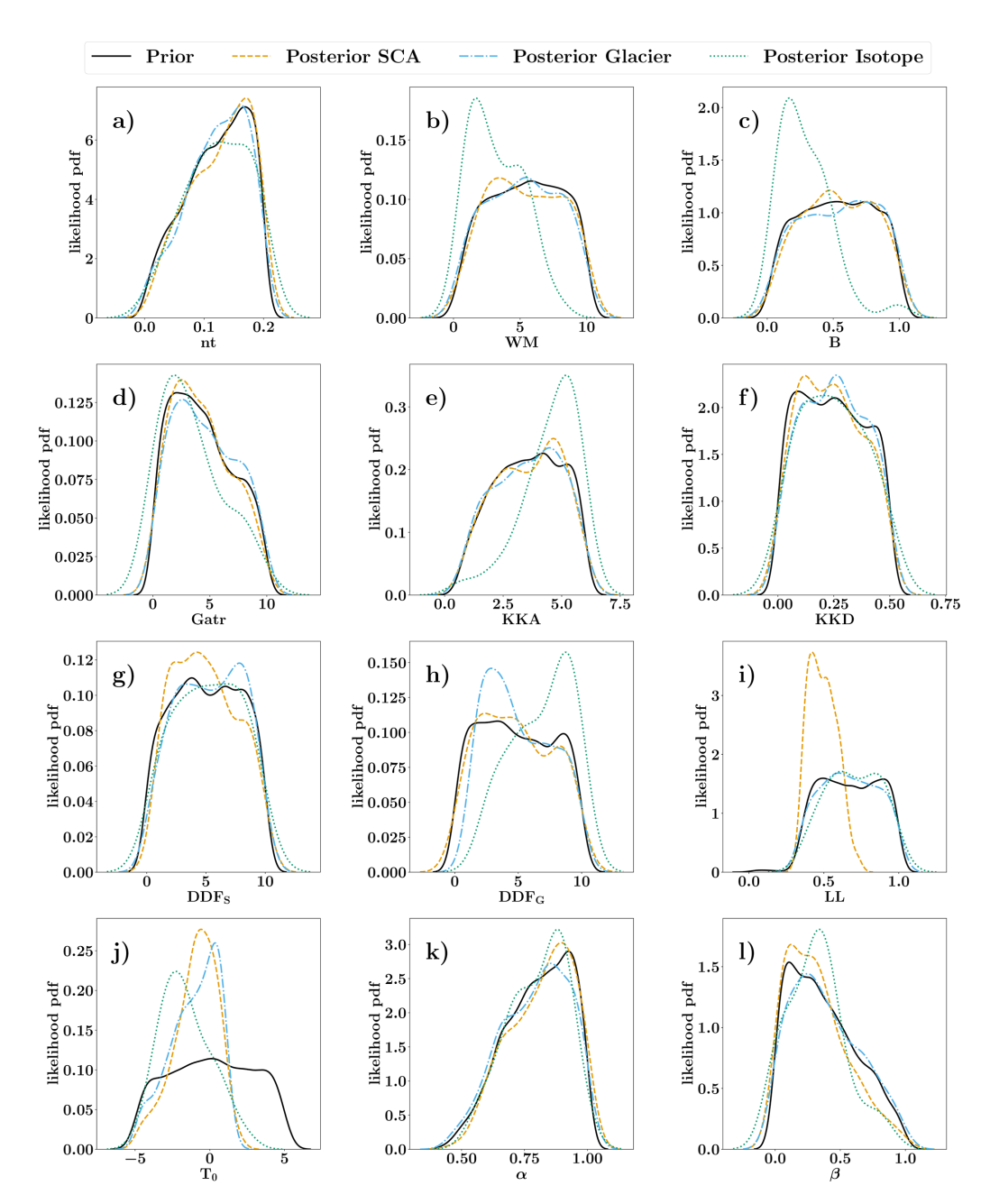


**Figure 4.** Parameter distributions obtained by conditioning the model with streamflow observations recorded at the Nuxia station (prior PDF, black line) and by combining streamflow measures with: (i) SCA (posterior PDF, orange dashed line); (ii) GMB (posterior PDF, light blue dash-dotted line); and (iii) isotope concentrations (posterior PDF, green dotted line).

the contrary, the most pronounced contraction of predictive uncertainty occurs during low-flow periods when the model is conditioned with isotopic data (Fig. 5e), whereas conditioning with SCA and GMB does not produce comparable reductions, Fig. 5a and c, respectively. In addition, FDCs, presented in the right-hand panels of Fig. 5, provide further insights into the effect of these datasets across different flow regimes. For SCA and GMB (Fig. 5b and d) the posterior uncertainty ranges are generally comparable to or slightly

narrower than the prior for medium-flow regimes. During low-flow conditions, however, the posterior bands are wider than the prior, indicating that incorporating SCA and GMB datasets introduces additional variability in streamflow predictions during low flow dominated periods, probably due to challenges in accurately constraining slow-response hydrological processes. For medium- and high-flow regimes, these datasets appear to modestly refine or maintain predictive uncertainty. In contrast, conditioning the model with isotopic

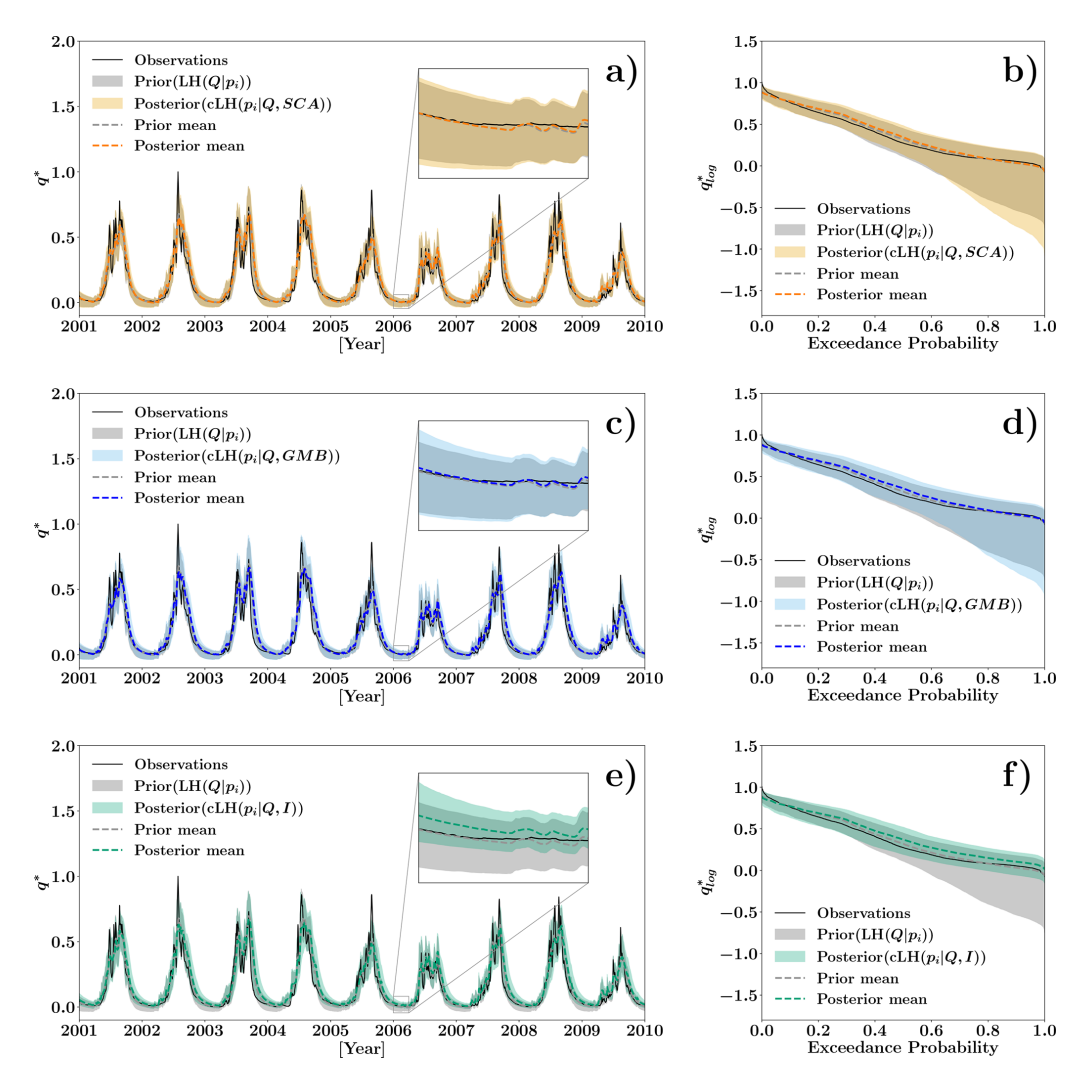


Figure 5. The 5%–95% percentile prior, conditioned solely on streamflow, and posterior predictive uncertainty ranges for streamflow, calculated under different conditions: SCA, GMB, and isotopes (I). Panels (a), (c), and (e) show daily streamflow time series for the period 2010–2015, with insets highlighting low-flow dynamics; panels (b), (d), and (f) show FDCs for the full period 2001–2015. Streamflow data are presented in dimensionless form owing to dissemination restrictions imposed by the data provider. A linear normalization,  $q^* = (Q - Q_{\min})/(Q_{\max} - Q_{\min})$ , is applied to the time series (a, c, e), while a logarithmic normalization,  $q^*_{\log} = (\log Q - \log Q_{\min})/(\log Q_{\max} - \log Q_{\min})$ , is used for the FDCs (b, d, f). In both cases,  $Q_{\min}$  and  $Q_{\max}$  refer to the minimum and maximum observed discharges at the Nuxia station.

data (Fig. 5f) results in a significant reduction in uncertainty, particularly during low-flow conditions. In contrast, conditioning the model with isotopic data (Fig. 5f) results in a significant reduction in uncertainty, particularly during low-flow conditions. The posterior uncertainty range is substantially narrower than the prior, indicating improved model consistency in simulating low flow dominated periods.

To further enhance interpretability and provide a deterministic reference alongside the probabilistic representation, Fig. 5 includes the mean simulated streamflow trajectories for both the prior and posterior distributions, in addition to the uncertainty bands and observed data. As evident from the figure insets and the FDCs, the prior and posterior means ex-

hibit slight differences across all cases, with a more noticeable divergence of the posterior mean from the prior in the case of isotope conditioning.

These patterns of uncertainty reduction – particularly the distinct effect of isotopic data during low-flow periods – are also evident at the Yangcun and Nugesha stations (Figs. S6 and S7 in the Supplement), further supporting the conclusions presented above. To facilitate a direct comparison of streamflow magnitude across the three stations, Fig. S8 in the Supplement provides time series and FDCs of normalized streamflow for the period 2001–2010. Note that any apparent loss of fit at the interior stations primarily reflects the fact that these sites (Yangcun and Nugesha) were not used

for parameter selection. In other words, parameter sets were derived at Nuxia and then transferred without adjustment to these upstream gauges. As a result, performance at Yangcun and Nugesha is affected by suboptimal parameter configurations. This loss of accuracy is consistent with previous findings (e.g., Khakbaz et al., 2012; Demirel et al., 2024), which show that applying parameters calibrated at a single location to different location of the basin, without re-evaluating them locally, lead to reduced model performance.

# 3.4 Runoff component analysis

Figure 6 shows the CRC produced by different behavioral parameter sets. The boxplots illustrate the contributions of the four runoff components under the prior parameter set and the posterior parameter sets constrained by SCA, GMB, and isotope likelihoods. The contributions of subsurface runoff and rainfall surface runoff are similar, both accounting for approximately 40 %–45 % of the total runoff (Fig. 6a and b). In contrast, snowmelt surface runoff and glacier melt surface runoff contribute approximately 8 % and 6 %, respectively (Fig. 6c and d). The estimated contributions of snowmelt and glacier melt are lower than some previous estimations in the study area (Boral and Sen, 2020; Lutz et al., 2014), but are close to some recent studies constraining the CRC estimation based on multiple datasets (Nan et al., 2025; Zhang et al., 2025; Chen et al., 2017).

The differences in the average CRCs among the parameter sets are relatively small, with variations generally below 3 % for all four components. However, the inferences drawn from the different datasets reveal interesting patterns regarding uncertainty reduction. The prior leads to a wider distribution of contributions across all runoff components, reflecting higher uncertainty in the model predictions. Posterior parameter sets constrained by specific datasets help reduce this uncertainty to varying extents. Constraining the model with the likelihood of GMB leads to a significant reduction in the uncertainty of glacier melt surface runoff (Fig. 6d), as evidenced by the tighter interquartile range and fewer outliers in the box plot. This indicates that the GMB simulation provides strong constraints on glacier-related processes. In contrast, the SCA does not lead to a significant reduction in the uncertainty of snowmelt surface runoff (Fig. 6c). This is because SCA data only constrains the area of snow but does not provide much constraint on the volume of snow, as the snow area-volume relation is determined by a calibrated parameter. Notably, the isotope likelihood demonstrates a broader impact on reducing uncertainty across multiple runoff components. The boxplots for I show narrower distributions for subsurface runoff, rainfall surface runoff, and snowmelt surface runoff, indicating that isotope simulation provides valuable constraints on both surface and subsurface hydrological processes.

The influence of each dataset on CRC uncertainties can be further illustrated by the result of sensitivity analysis, which evaluates the extent to which each performance metric is influenced by the contribution of each runoff component. To this end, Fig. 7 presents the sensitivity of model performance metrics to the contributions of different runoff components, namely, subsurface runoff ( $C_{\rm ss}$ ), rainfall surface runoff ( $C_{\rm sr}$ ), snowmelt surface runoff ( $C_{\rm sm}$ ), and glacier melt surface runoff ( $C_{\rm sgm}$ ). The sensitivity analysis evaluates the extent to which each performance metric – streamflow NSE $_Q$ , SCA NSE $_{\rm SCA}$ , GMB VE $_{\rm GMB}$ , and isotope NSE $_{\rm I}$  – is influenced by the relative contribution of each runoff component to total streamflow.

The results indicate that streamflow performance  $NSE_Q$ and SCA performance NSE<sub>SCA</sub> respond differently to variations in the contribution of individual runoff components. While NSE<sub>SCA</sub> remains largely insensitive to CRC variations, showing consistently high values across a wide range of runoff component contributions, NSE<sub>Q</sub> exhibits a more noticeable response. The scatterplots reveal that although streamflow performance remains relatively high (NSE<sub>O</sub> > 0.8) even when CRC deviates from its optimal value, there is a clear tendency for behavioral solutions to cluster towards an optimal CRC, indicating a degree of sensitivity. In contrast, GMB performance VE<sub>GMB</sub> shows strong sensitivity to glacier melt runoff  $C_{\text{sgm}}$ , with  $VE_{\text{GMB}}$  dropping significantly when  $C_{\rm sgm}$  exceeds approximately 10 %. The most pronounced sensitivity is observed in the isotope performance metric NSE<sub>I</sub>, which responds to variations in multiple runoff components. The scatterplots reveal that NSE<sub>I</sub> declines markedly when the contributions of subsurface runoff  $C_{\rm ss}$ , rainfall runoff  $C_{\rm sr}$ , or snowmelt runoff  $C_{\rm sm}$  deviate from optimal values. In particular, NSE<sub>I</sub> decreases significantly from 0.4 to below 0.2 when the contributions of these components shift, indicating that isotopic simulations are much more sensitive to changes in runoff contributions compared to other performance metrics. This sensitivity underscores the importance of accurately quantifying the partitioning of different runoff components to achieve reliable isotopebased model predictions. Overall, the analysis highlights that VE<sub>GMB</sub> simulations are primarily sensitive to glacier melt runoff, whereas isotope-based simulations NSE<sub>I</sub> are more sensitive to a broader range of runoff components.

Note that, although NSE is not ideally suited to capture spatial features of snow cover dynamics, our analysis focuses on the catchment-integrated SCA, for which NSE remains an informative metric to evaluate the agreement between observed and simulated temporal patterns of areal extent. In this regard, to better assess model performance, we provide the time series of observed versus simulated SCA in Fig. S3 in the Supplement, along with corresponding comparisons for GMB and isotopic signatures in Figs. S4 and S5 in the Supplement. These visualizations allow the reader to evaluate the temporal evolution and potential systematic biases for each variable, together with the associated posterior predictive uncertainty ranges for SCA, GMB, and isotopic data.

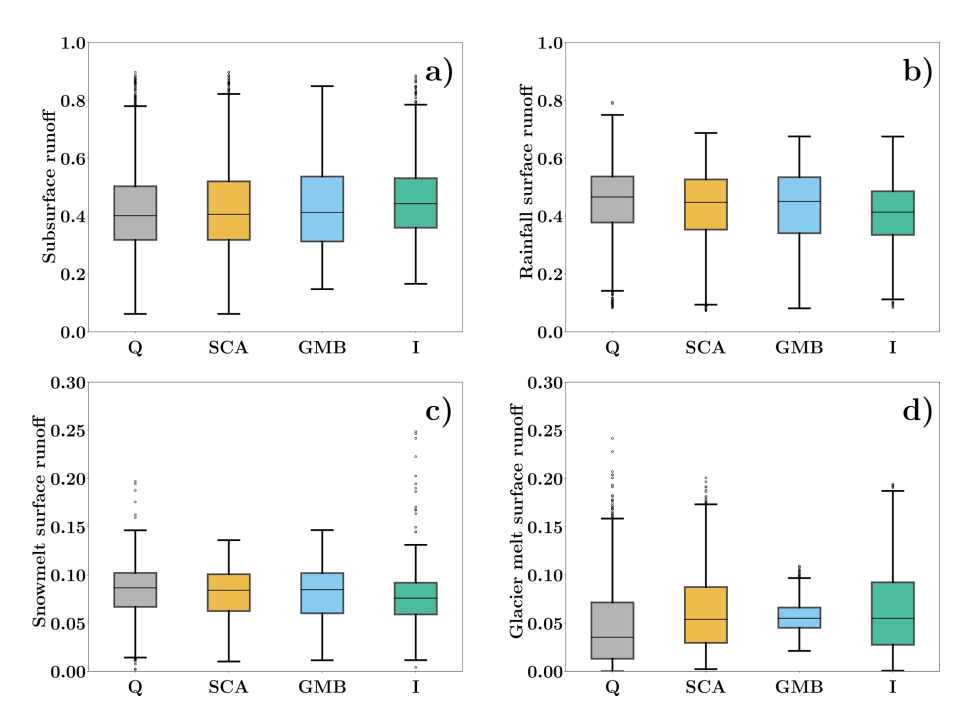


**Figure 6.** Boxplots showing the variability in the contributions of different surface runoff components under prior estimates conditioned solely on streamflow (Q) and posterior estimates conditioned on additional datasets: SCA, GMB, and isotopic data (I). Panel (a): Subsurface runoff; panel (b): rainfall surface runoff; panel (c): Snowmelt surface runoff; panel (d): glacier melt runoff.

#### 4 Discussion

Overall, the results presented in Sect. 3 highlight the differential value of auxiliary datasets in hydrological model calibration. While SCA and GMB provide insights into snow and glacier dynamics, they appear less effective in reducing streamflow uncertainty. Not only do the results prove that integrating multiple data sources within the Bayesian framework influences both streamflow simulation uncertainties and the computation of CRC components, but they also show varying effects depending on the type of dataset and runoff component considered, as discussed below.

# 4.1 Reducing streamflow model uncertainty using a Bayesian framework

The results of this study differ in another perspective from those of Di Marco et al. (2021), who observed a consistent relationship in snow-dominated basins between an increased likelihood of streamflow and SCA, alongside a reduction in streamflow uncertainty. In contrast, our findings do not show a comparable narrowing of streamflow uncertainty bands when applying the Bayesian filtering approach with snow and glacier parameters (Fig. 5). This discrepancy suggests that the coupling between snow and glacier dynamics and streamflow performance is not straightforward, particularly in larger or more heterogeneous catchments.

As noted by Ruelland (2024), the potential for snow data to enhance streamflow simulation consistency and robustness depends on various factors, including hydro-climatic conditions, spatial variability, the modeling framework, and the accuracy of snow cover data (Hao et al., 2022) and input forcing (Raleigh et al., 2015). Factors such as catchment complexity, spatial heterogeneity, and structural uncertainties in the model, stemming from unresolved hydrological processes or oversimplified dynamics, probably contribute to the persistence of wide uncertainty ranges. In contrast, isotopic likelihoods effectively constrain the parameter space, resulting in improved simulation performance and reduced uncertainty bands, particularly during low-flow conditions. This finding confirms the ability of isotopic data to capture key hydrological processes, such as groundwater-surface water mixing and subsurface flow dynamics, which are especially influential during low-flow periods (Jasechko and Taylor, 2015), where seasonality plays a critical role (Birkel et al., 2009).

The influence of hydrological processes seasonality on the effectiveness of likelihoods is demonstrated by the sharpness polar plot (Fig. 8). This figure illustrates the SH ranges for posterior likelihoods conditioned on SCA, GMB, and I datasets throughout the year. A maximum SH value of 0.34 was observed for isotopes on 16 March 2008, while the maximum SH values for SCA and GMB were 0.19 on 30 April 2009, and 0.16 on 10 June 2009, respectively. These results highlight the effectiveness of isotopic likelihoods during winter and early spring, with SH values remaining consistently narrow and never dropping below zero, a period when the model indicates a predominance of contributions

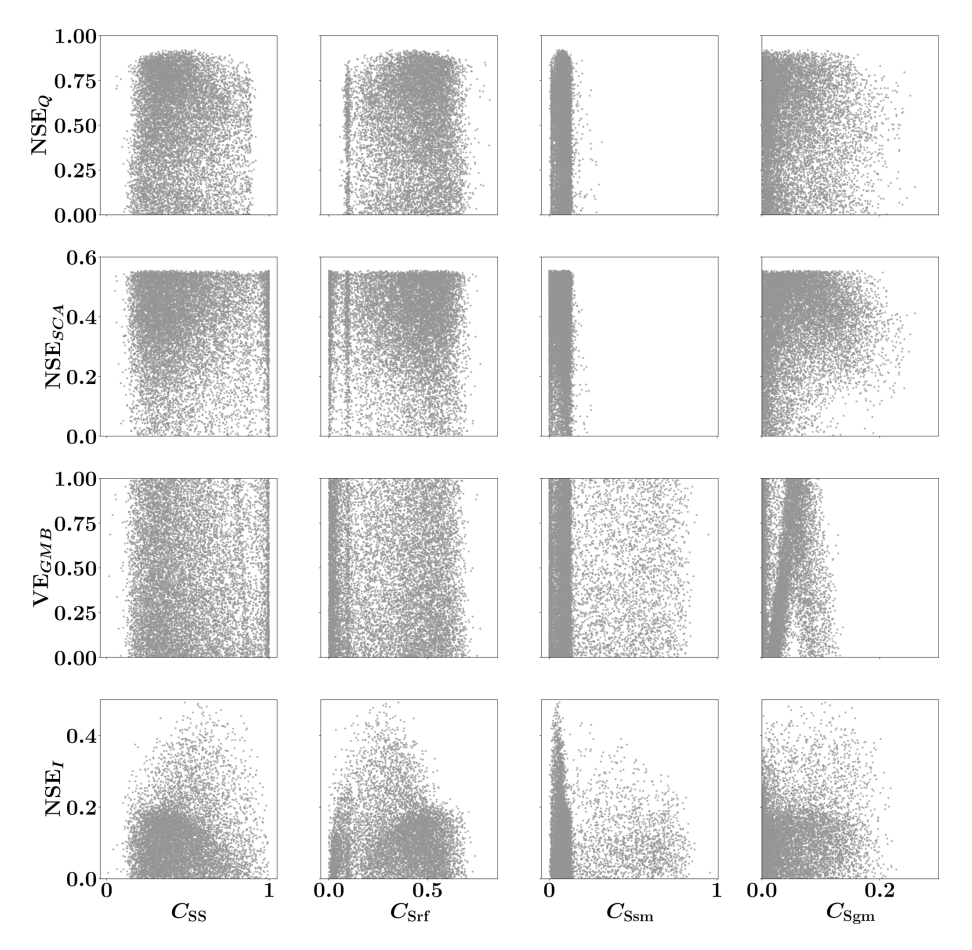


**Figure 7.** Sensitivity of model performance metrics to runoff component contributions: streamflow NSE<sub>Q</sub>, SCA NSE<sub>SCA</sub>, GMB VE<sub>GMB</sub>, and isotopes NSE<sub>I</sub>, plotted against subsurface runoff ( $C_{ss}$ ), rainfall surface runoff ( $C_{sr}$ ), snowmelt surface runoff ( $C_{sm}$ ), and glacier melt surface runoff ( $C_{sgm}$ ). Each point represents a behavioral solution from the multi-objective calibration.

from the subsurface flow component. In contrast, SCA and GMB likelihoods achieve their SH peaks during spring and early summer, coinciding with periods of rapid snowmelt and glacier runoff. This pattern underscores the importance of integrating SCA and GMB likelihoods for capturing highflow dynamics and highlights the need to further develop these datasets to enhance their effectiveness in constraining streamflow uncertainty during these critical periods.

At this point, it is important to recall that SH refers to the degree of concentration of the ensemble simulations where a sharper ensemble has a narrower spread, indicating higher predictive confidence (Gneiting et al., 2007). However, increased SH does not necessarily translate into improved reliability. In our case, the inclusion of isotopic data led to a more constrained ensemble, resulting in a sharper posterior distribution of streamflow simulations. While this outcome reflects the stronger constraining power of isotopic information, it also increased the likelihood that observed values fall outside the model's predictive bounds, thereby reducing the CR. Compared to calibrations using SCA or GMB, the sharper ensemble derived from isotope-informed calibration

was less able to fully capture observed variability. This illustrates the classic trade-off between predictive confidence and reliability – in other words, between SH and CR in probabilistic modeling (Beven and Binley, 1992), and emphasizes the need to balance these aspects when evaluating ensemble-based hydrological simulations.

These results confirm that isotopic data are highly effective in reducing model uncertainty by providing independent constraints on flow partitioning and subsurface processes. However, to translate this enhanced internal consistency into improved predictive coverage, future research should explore model structural refinements that better align SH with CR. Furthermore, these findings illustrate both the potential and the limitations of Bayesian inference in simultaneously capturing fast surface runoff and slower subsurface dynamics. Although SH values demonstrate its capacity to constrain parameter uncertainty across diverse hydrological processes, alternative calibration strategies, such as multi-objective weighted optimization, may offer additional improvements in streamflow simulation accuracy (He et al., 2019). Still, the sensitivity of model outputs to weight selec-

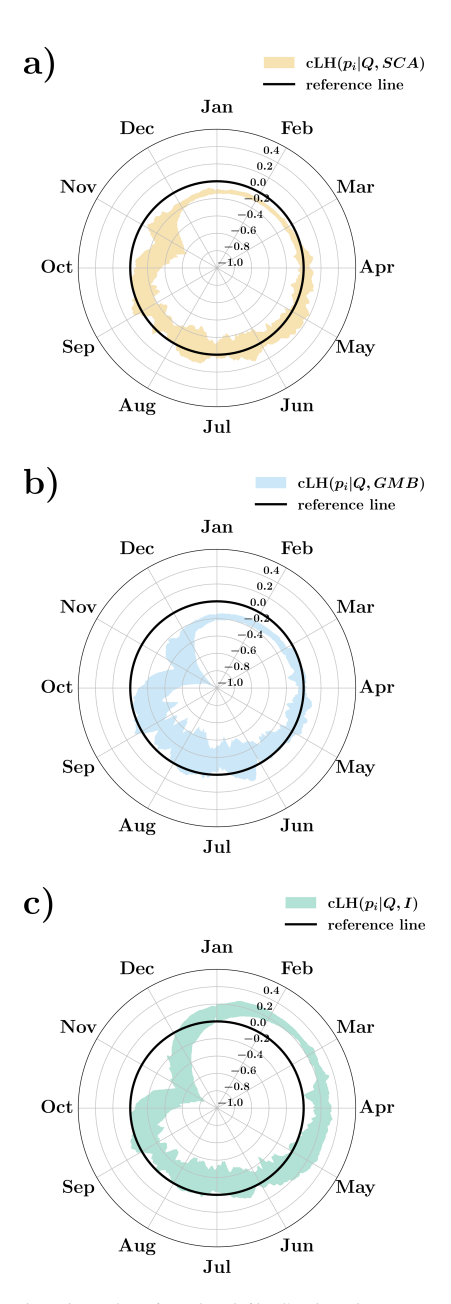


**Figure 8.** Polar plots showing the daily SH band computed from the maximum and minimum SH values across the years 2010–2015. The shaded regions represent the range of SH variability for each day of the year, while the solid black line indicates the reference level at zero SH. The subplots illustrate the SH calculated under different conditioning:  $cLH(p_i|Q,SCA)$  (a),  $cLH(p_i|Q,GMB)$  (b), and  $cLH(p_i|Q,I)$  (c).

tion necessitates careful application (Tong et al., 2021, 2022). Finally, the interplay between likelihood functions underscores the metric-dependent nature of parameter uncertainty reduction and the value of integrating multiple complementary evaluation criteria during calibration (e.g., Fenicia et al., 2018; Majone et al., 2022).

These results also point to the need for improved coupling and integration of individual model components. Such integration would allow for better exploitation of the strengths of each dataset and enhance the Bayesian framework's capability to constrain parameter ranges across diverse hydrological conditions. By addressing these structural connections and leveraging synergies between complementary metrics, the Bayesian framework's potential to optimize parameter calibration and improve predictive accuracy can be fully realized.

In this context, the posterior mean streamflow, especially in the isotope-conditioned simulations, fails to consistently outperform the prior mean streamflow in reproducing the observed discharge, despite exhibiting narrower uncertainty bands in some streamflow regimes (see Sect. 3). This deterioration in deterministic skill is not unexpected. Previous studies (e.g., Vrugt and Sadegh, 2013; Botto et al., 2018) have shown that reducing ensemble spread does not automatically lead to improved agreement with observations. Structural model deficiencies and varying accuracy of input data sources (i.e., SCA, GMB, and I) may introduce systematic posterior bias, since the conditioning step attempts to compensate for processes that are poorly captured by the model or affected by different levels of uncertainty (Beven and Freer, 2001; Chowdhury and Sharma, 2007).

It is important to emphasize that the ensemble mean does not correspond to the best-performing simulation in terms of NSE, and may smooth out dynamic features that are better reproduced by individual ensemble members. Moreover, the goal of the data-conditioning approach is not to maximize deterministic skill, but rather to reduce predictive uncertainty by constraining the prior ensemble: the shift from prior to posterior aims at narrowing the uncertainty bands of the streamflow simulations, even at the cost of some loss in individual accuracy (Beven, 2006).

#### 4.2 Runoff component uncertainty

The GMB dataset effectively reduces uncertainty in glacier melt surface runoff simulations (Fig. 6d), emphasizing its value for improving model constraints in glacier-dominated systems. This finding aligns with previous studies highlighting the importance of incorporating GMB data to enhance streamflow predictions in such catchments (Stahl et al., 2008; O'Neel et al., 2014; Yang et al., 2024). However, this reduction in uncertainty does not always translate into improved streamflow predictions at the basin scale. The effectiveness of the Bayesian framework in reducing uncertainties depends on the proportion of runoff attributed to glacier melt processes. Consequently, even when glacier-related dynamics is well constrained by GMB data, its contribution to reducing overall streamflow prediction uncertainty may be limited in basins where other processes dominate. This underscores the importance of considering basin scale and dominant runoff processes when selecting datasets for hydrological modeling.

Similarly, SCA datasets provide valuable constraints on snowmelt surface runoff (Fig. 6c) but have a more limited impact on reducing streamflow uncertainty. This may be due to the spatial and temporal resolution limitations of SCA datasets (Di Marco et al., 2020), or because the snowmelt contribution to total runoff is relatively minor in large basins compared to other components, such as subsurface runoff and rainfall surface runoff. Furthermore, uncertainties in the timing and rate of snowmelt, which are critical for runoff generation, may not be fully captured by remotely sensed SCA data (Dietz et al., 2012). This limitation is particularly relevant in basins with complex snow dynamics, where snow cover depletion varies significantly across different elevation bands and time periods (Molotch and Margulis, 2008).

In contrast, isotopic data stand out for their ability to reduce uncertainty across multiple runoff components, particularly during low-flow conditions. By tracing water sources and pathways, isotopic tracers provide critical insights into subsurface and groundwater contributions, which are difficult to capture with traditional datasets (Birkel et al., 2015). Isotopic tracers, such as oxygen-18 ( $\delta^{18}$ O) and deuterium (D), are widely used to distinguish between recent precipitation, snowmelt, and groundwater contributions to streamflow, improving the calibration of hydrological models (Jasechko, 2019). Our results show that the isotope data does not reduce the uncertainty of glacier melt runoff, because the model assumes that glacier melt generates runoff directly through surface pathway, not involved in the surfacesubsurface runoff partitioning, the aspect for which isotopic data are most useful. The results suggest that incorporating isotopic data into hydrological models can help reduce uncertainties related to water source contributions and flow pathways, particularly in catchments with complex surfacesubsurface interactions. Such benefit comes from the significant divergence in the isotope signatures of surface and subsurface runoff, i.e., a much lower temporal variability of groundwater isotope compared to surface runoff because of the long travel time.

These differences in the influence of datasets underscore the importance of selecting appropriate data sources based on the specific hydrological processes and uncertainties that need to be addressed in a given catchment. For example, GMB data should be prioritized in glacier-fed basins to improve predictions of glacier melt runoff (Huss and Hock, 2015), whereas isotope data can provide valuable constraints on multiple runoff components, particularly in catchments with diverse flow generation processes (Rodgers et al., 2005; Birkel et al., 2011). The integration of multi-source datasets can help reduce model uncertainties more effectively than relying on a single dataset (Beven, 2006), resulting in more robust predictions of water availability and streamflow variability under changing climatic conditions (Borriero et al., 2023).

#### 4.3 Limitations

This study systematically evaluates the value of SCA, GMB, and isotopes in reducing model uncertainties. Results highlight the critical role of isotope data in improving low-flow simulations and runoff component separation. However, several limitations persist. First, while streamflow simulations achieve NSE values up to 0.9, peak flows are consistently underestimated, probably owing to inaccuracies in precipitation forcing data (Jiang et al., 2022; Xu et al., 2017). Metrics for SCA and isotope simulations remain around 0.5, indicating potential for further optimization. Second, the model structure is rather simplified when conceptualizing processes such as groundwater and snow/ice melting. Specifically, only two subsurface layers (u-zone and s-zone in the model) are defined, and the subsurface outflows are simulated as a sum. Only the shallow groundwater processes are considered, only occurring within each REW, which is unable to adequately describe subsurface processes in the TP, where deep interbasin groundwater pathways exist (Chen et al., 2025). Meanwhile, the simple degree-day factor method was used to simulate the melting processes, to make the model adequately efficient for subsequent GLUE analysis. These modules can be improved to strengthen the physical basis of the model. Third, as this analysis is based on a single case study in a specific region, its broader applicability is uncertain. Unlike prior studies (Di Marco et al., 2021; Tong et al., 2021), snow and glacier datasets did not significantly enhance model performance here, suggesting the need to clarify the conditions under which such data prove most beneficial.

Despite these challenges, the study underscores the importance of employing multiple datasets to constrain hydrological models. Although snow and glacier datasets alone may not substantially improve streamflow simulations, they are essential for ensuring model reliability in capturing key processes. Isotope data, in particular, effectively constrain surface and subsurface runoff separation owing to the low variability in groundwater I (Nan et al., 2024; McGuire and McDonnell, 2006), reducing low flow uncertainties and enhancing model robustness.

### 5 Conclusions

This study provides new insights into reducing uncertainty and equifinality in the hydrological modeling of large mountainous catchments by integrating multiple auxiliary datasets within a Bayesian framework. By systematically comparing the contributions of SCA, GMB, and isotopic tracers, we demonstrate how these datasets distinctly improve model performance across various flow regimes.

A critical conclusion drawn from this research is the unique advantage of isotopic data in reducing model uncertainty during low-flow periods. The isotopic likelihood has shown to be more effective in constraining subsurface

flow contributions and groundwater—surface water interactions, resulting in narrower uncertainty ranges for streamflow predictions under low-flow conditions. This finding underscores the critical role of isotopic tracers in improving the representation of slow-response hydrological processes, which are essential for the mitigation of drought and sustainable management of water resources in mountainous regions. In contrast, the SCA and GMB datasets were found to be more effective in capturing rapid surface dynamics, such as snowmelt and glacier melt processes. However, their contributions to reducing streamflow uncertainty were limited, particularly during low-flow conditions. This discrepancy highlights the need for multi-objective calibration approaches that balance the trade-offs between rapid surface responses and slow subsurface processes.

Our results also reveal the differential impact of each dataset on the CRC. The GMB likelihood significantly reduces uncertainty in glacier melt surface runoff, whereas isotopic data provide broader constraints across multiple runoff components, including subsurface runoff, rainfall surface runoff, and snowmelt surface runoff. These differences emphasize the importance of selecting appropriate datasets based on the dominant hydrological processes in a given catchment.

The study further highlights the limitations of current Bayesian frameworks in fully leveraging the complementary strengths of auxiliary datasets. While Bayesian approaches are effective in reducing parameter uncertainty and improving model calibration, the persistent wide uncertainty ranges for streamflow predictions indicate the need for improved coupling and integration of individual model components. Enhancing these structural connections within the modeling framework could allow for better exploitation of multisource datasets, ultimately improving predictive accuracy across diverse hydrological conditions.

In conclusion, our findings stress the importance of incorporating multi-source datasets in hydrological modeling to achieve robust performance across different flow regimes. The integration of isotopic tracers, snow cover, and GMB data within a Bayesian framework offers a promising pathway to reduce uncertainty and enhance the understanding of streamflow variability in large mountainous catchments. Future research should focus on developing more advanced coupling methods that account for the complex interplay between cryospheric and subsurface processes, as well as exploring the potential of multi-objective weighted calibration approaches to further improve model reliability.

Code availability. The THREW-T model code used in this study is available from the corresponding author (ny1209@qq.com).

Data availability. Data sets are publicly available as follows: DEM (http://www.gscloud.cn/sources/details/310?pid=302,

last access: 1 January 2019, Geospatial Data Cloud Site, 2019), CMFD (China Meteorological Forcing Data, https://doi.org/10.11888/AtmosphericPhysics.tpe.249369.file, Yang and He, 2019), glacier inventory data (https://doi.org/10.3972/glacier.001.2013.db, Liu, 2012), glacier elevation change data (https://doi.org/10.6096/13, Hugonnet et al., 2021), **NDVI** (https://doi.org/10.5067/MODIS/MOD13A3.006, Didan. 2015), LAI (https://doi.org/10.5067/MODIS/MOD15A2H.006, Myneni et al., 2015), HWSD (Harmonized World Soil Database, https://data.tpdc.ac.cn/zh-hans/data/ 3519536a-d1e7-4ba1-8481-6a0b56637baf/?q=HWSD, He, 2019). The simulated streamflow, SCA, GMB and isotope data produced by the behavioral parameters and the 5th–95th streamflow uncertainty bands for both the prior and posterior ensembles are provided on Zenodo at https://zenodo.org/records/15605202 (Nan and Avesani, 2025a) and https://zenodo.org/records/16634369 (Nan and Avesani, 2025b). The datasets not publicly available are referred to in the main text (Chen et al., 2018; Liu et al., 2007).

*Supplement.* The supplement related to this article is available online at https://doi.org/10.5194/hess-29-5755-2025-supplement.

Author contributions. DA was responsible for conceiving the study; developing the methodology; acquiring funding; carrying out the investigation; developing the software; preparing, reviewing, and editing the manuscript; and supervising the study. YN conceived the study, contributed to developing the software, carrying out the investigation, creating the figures, curating the data, and reviewing and editing the manuscript; FT reviewed and edited the manuscript, and supervised the study.

Competing interests. At least one of the (co-)authors is a member of the editorial board of *Hydrology and Earth System Sciences*. The peer-review process was guided by an independent editor, and the authors also have no other competing interests to declare.

Disclaimer. Publisher's note: Copernicus Publications remains neutral with regard to jurisdictional claims made in the text, published maps, institutional affiliations, or any other geographical representation in this paper. While Copernicus Publications makes every effort to include appropriate place names, the final responsibility lies with the authors. Views expressed in the text are those of the authors and do not necessarily reflect the views of the publisher.

Acknowledgements. During the preparation of this work, the authors used ChatGPT in order to improve language and readability of the original draft, with caution. After using these tools, the authors reviewed and edited the content as needed and take full responsibility for the content of the publication. This study was supported by the National Natural Science Foundation of China (grant no. 52309023) and the Fund Program of State Key Laboratory of Hydroscience and Engineering (sklhseTD-2024-C01). Diego Avesani acknowledges the Italian Ministry of Education, Universities and

Research (MUR), in the framework of the project DICAM-EXC [Departments of Excellence 2023–2027, grant L232/2016], and the support from the European Union – FSE-REACT-EU, PON Research and Innovation 2014–2020 DM1062/2021, PAT Project Drought Indicators – CUP C97G22000460003. The open-access publication of this study is supported by the Fund Program of State Key Laboratory of Hydroscience and Engineering (sklhseTD-2024-C01).

Financial support. This study was supported by the National Natural Science Foundation of China (grant nos. 52579012 and 52309023) and the Fund Program of the State Key Laboratory of Hydroscience and Engineering (sklhseTD-2024-C01). The openaccess publication is supported by the National Natural Science Foundation of China (grant no. 52579012).

Review statement. This paper was edited by Markus Hrachowitz and reviewed by three anonymous referees.

#### References

- Andraos, C.: Breaking Uncertainty Barriers: Approximate Bayesian Computation Advances in Rainfall–Runoff Modeling, Water, 16, https://doi.org/10.3390/w16233499, 2024.
- Araya, D., Mendoza, P. A., Muñoz-Castro, E., and McPhee, J.: Towards robust seasonal streamflow forecasts in mountainous catchments: impact of calibration metric selection in hydrological modeling, Hydrol. Earth Syst. Sci., 27, 4385–4408, https://doi.org/10.5194/hess-27-4385-2023, 2023.
- Asong, Z. E., Elshamy, M. E., Princz, D., Wheater, H. S., Pomeroy, J. W., Pietroniro, A., and Cannon, A.: High-resolution meteorological forcing data for hydrological modelling and climate change impact analysis in the Mackenzie River Basin, Earth Syst. Sci. Data, 12, 629–645, https://doi.org/10.5194/essd-12-629-2020, 2020.
- Betterle, A. and Bellin, A.: Morphological and Hydrogeological Controls of Groundwater Flows and Water Age Distribution in Mountain Aquifers and Streams, Water Resources Research, 60, e2024WR037407, https://doi.org/10.1029/2024WR037407, 2024.
- Beven, K.: A manifesto for the equifinality thesis, Journal of Hydrology, 320, 18–36, https://doi.org/10.1016/j.jhydrol.2005.07.007, 2006.
- Beven, K. and Freer, J.: Equifinality, data assimilation, and uncertainty estimation in mechanistic modelling of complex environmental systems using the GLUE methodology, Journal of Hydrology, 249, 11–29, https://doi.org/10.1016/S0022-1694(01)00421-8, 2001.
- Beven, K. J. and Binley, A. M.: The future of distributed models: Model calibration and uncertainty prediction, Hydrological Processes, 6, 279–298, https://doi.org/10.1002/hyp.3360060305, 1992.
- Birkel, C., Tetzlaff, D., and Dunn, S.: Towards a simple dynamic process conceptualization in rainfall-runoff models using multi-criteria calibration and tracers in temper-

- ate, upland catchments, Hydrological Processes, 24, 260–275, https://doi.org/10.1002/hyp.7478, 2009.
- Birkel, C., Soulsby, C., Tetzlaff, D., and Malcolm, I. A.: Modelling catchment-scale water storage dynamics: Reconciling dynamic storage with tracer-inferred passive storage, Hydrological Processes, 25, 3924–3936, https://doi.org/10.1002/hyp.8201, 2011.
- Birkel, C., Soulsby, C., Tetzlaff, D., and Dunn, S. M.: Developing a tracer-aided rainfall-runoff model to simulate hydrological processes in mesoscale catchments, Water Resources Research, 50, 944–961, https://doi.org/10.1002/2013WR014925, 2014.
- Birkel, C., Soulsby, C., and Tetzlaff, D.: Integrating parsimonious models of hydrological connectivity and soil biogeochemistry to simulate stream DOC dynamics, Water Resources Research, 51, 2541–2557, https://doi.org/10.1002/2013JG002551, 2015.
- Blasone, R.-S., Vrugt, J. A., Madsen, H., Rosbjerg, D., Robinson, B. A., and Zyvoloski, G. A.: Generalized likelihood uncertainty estimation (GLUE) using adaptive Markov Chain Monte Carlo sampling, Advances in Water Resources, 31, 630–648, https://doi.org/10.1016/j.advwatres.2007.12.003, 2008.
- Boral, S. and Sen, I. S.: Tracing "Third Pole" ice meltwater contribution to the Himalayan rivers using oxygen and hydrogen isotopes, Geochemical Perspectives Letters, 48–53, https://doi.org/10.7185/geochemlet.2013, 2020.
- Borriero, A., Kumar, R., Nguyen, T. V., Fleckenstein, J. H., and Lutz, S. R.: Uncertainty in water transit time estimation with StorAge Selection functions and tracer data interpolation, Hydrol. Earth Syst. Sci., 27, 2989–3004, https://doi.org/10.5194/hess-27-2989-2023, 2023.
- Botto, A., Belluco, E., and Camporese, M.: Multi-source data assimilation for physically based hydrological modeling of an experimental hillslope, Hydrol. Earth Syst. Sci., 22, 4251–4266, https://doi.org/10.5194/hess-22-4251-2018, 2018.
- Brazier, R. E., Beven, K. J., Freer, J., and Rowan, J. S.: Equifinality and uncertainty in physically based soil erosion models: application of the GLUE methodology to WEPP the Water Erosion Prediction Project for sites in the UK and USA, Earth Surface Processes and Landforms, 25, 825–845, https://doi.org/10.1002/1096-9837(200008)25:8<825::AID-ESP101>3.0.CO;2-3, 2000.
- Chang, Z., Gao, H., Yong, L., Wang, K., Chen, R., Han, C., Demberel, O., Dorjsuren, B., Hou, S., and Duan, Z.: Projected future changes in the cryosphere and hydrology of a mountainous catchment in the upper Heihe River, China, Hydrol. Earth Syst. Sci., 28, 3897–3917, https://doi.org/10.5194/hess-28-3897-2024, 2024.
- Chen, J., Kuang, X., Fan, L., and Zheng, C.: Interbasin groundwater flows in the Yarlung Zangbo River Basin and its surrounding areas: A perspective, Science China-Technological Sciences, 68, https://doi.org/10.1007/s11431-024-2845-0, 2025.
- Chen, X., Long, D., Hong, Y., Zeng, C., and Yan, D.: Improved modeling of snow and glacier melting by a progressive two-stage calibration strategy with GRACE and multisource data: How snow and glacier meltwater contributes to the runoff of the Upper Brahmaputra River basin?, Water Resources Research, 53, 2431–2466, https://doi.org/10.1002/2016wr019656, 2017.
- Chen, X., Long, D., Liang, S., He, L., Zeng, C., Hao, X., and Hong, Y.: Developing a composite daily snow cover extent record over the Tibetan Plateau from 1981 to 2016 using mul-

- tisource data, Remote Sensing of Environment, 215, 284–299, https://doi.org/10.1016/j.rse.2018.06.021, 2018.
- Chowdhury, S. and Sharma, A.: Mitigating parameter bias in hydrological modelling due to uncertainty in covariates, Journal of Hydrology, 340, 197–204, https://doi.org/10.1016/j.jhydrol.2007.04.010, 2007.
- Cui, T., Li, Y., Yang, L., Nan, Y., Li, K., Tudaji, M., Hu, H., Long, D., Shahid, M., Mubeen, A., He, Z., Yong, B., Lu, H., Li, C., Ni, G., Hu, C., and Tian, F.: Non-monotonic changes in Asian Water Towers' streamflow at increasing warming levels, Nature Communications, 14, https://doi.org/10.1038/s41467-023-36804-6, 2023.
- Dalla Torre, D., Di Marco, N., Menapace, A., Avesani, D., Righetti, M., and Majone, B.: Suitability of ERA5-Land reanalysis dataset for hydrological modelling in the Alpine region, Journal of Hydrology: Regional Studies, 52, 101718, https://doi.org/10.1016/j.ejrh.2024.101718, 2024.
- Demirel, M. C., Koch, J., Rakovec, O., Kumar, R., Mai, J., Müller, S., Thober, S., Samaniego, L., and Stisen, S.: Tradeoffs Between Temporal and Spatial Pattern Calibration and Their Impacts on Robustness and Transferability of Hydrologic Model Parameters to Ungauged Basins, Water Resources Research, 60, e2022WR034193, https://doi.org/10.1029/2022WR034193, 2024.
- Di Marco, N., Righetti, M., Avesani, D., Zaramella, M., Notarnicola, C., and Borga, M.: Comparison of MODIS and Model-Derived Snow-Covered Areas: Impact of Land Use and Solar Illumination Conditions, Geosciences, 10, https://doi.org/10.3390/geosciences10040134, 2020.
- Di Marco, N., Avesani, D., Righetti, M., Zaramella, M., Majone, B., and Borga, M.: Reducing hydrological modelling uncertainty by using MODIS snow cover data and a topography-based distribution function snowmelt model, Journal of Hydrology, 599, 126020, https://doi.org/10.1016/j.jhydrol.2021.126020, 2021.
- Didan, K.: MOD13A3 MODIS/Terra vegetation Indices Monthly L3 Global 1 km SIN Grid V006, NASA EOSDIS Land Processes DAAC [data set], https://doi.org/10.5067/MODIS/MOD13A3.006, 2015.
- Dietz, A. J., Kuenzer, C., Gessner, U., and Dech, S.: Remote sensing of snow a review of available methods, International Journal of Remote Sensing, 33, 4094–4134, https://doi.org/10.1080/01431161.2011.640964, 2012.
- Efstratiadis, A. and Koutsoyiannis, D.: One decade of multiobjective calibration approaches in hydrological modelling: a review, Hydrological Sciences Journal, 55, 58–78, https://doi.org/10.1080/02626660903526292, 2010.
- Fassnacht, S. R., Sexstone, G. A., Kashipazha, A. H., Ignacio Lopez-Moreno, J., Jasinski, M. F., Kampf, S. K., and Von Thaden, B. C.: Deriving snow-cover depletion curves for different spatial scales from remote sensing and snow telemetry data, Hydrological Processes, 30, 1708–1717, https://doi.org/10.1002/hyp.10730, 2016.
- Fenicia, F., Kavetski, D., Reichert, P., and Albert, C.: Signature-Domain Calibration of Hydrological Models Using Approximate Bayesian Computation: Empirical Analysis of Fundamental Properties, Water Resources Research, 54, 3958–3987, https://doi.org/10.1002/2017WR021616, 2018.
- Finger, D., Pellicciotti, F., Konz, M., Rimkus, S., and Burlando, P.: The value of glacier mass balance, satellite snow cover images,

- and hourly discharge for improving the performance of a physically based distributed hydrological model, Water Resources Research, https://doi.org/10.1029/2010WR009824, 2011.
- Franks, S. W., Gineste, P., Beven, K. J., and Merot, P.: On constraining the predictions of a distributed model: The incorporation of fuzzy estimates of saturated areas into the calibration process, Water Resources Research, 34, 787–797, https://doi.org/10.1029/97WR03041, 1998.
- Gan, Y., Liang, X.-Z., Duan, Q., Ye, A., Di, Z., Hong, Y., and Li, J.: A systematic assessment and reduction of parametric uncertainties for a distributed hydrological model, Journal of Hydrology, 564, 697–711, https://doi.org/10.1016/j.jhydrol.2018.07.055, 2018.
- Geospatial Data Cloud Site: ASTER GDEM 30M, Geospatial Data Cloud Site [data set], http://www.gscloud.cn/sources/details/310?pid=302 (last access: 1 January 2019), 2019.
- Gneiting, T., Balabdaoui, F., and Raftery, A. E.: Probabilistic forecasts, calibration and sharpness, Journal of the Royal Statistical Society: Series B (Statistical Methodology), 69, 243–268, https://doi.org/10.1111/j.1467-9868.2007.00587.x, 2007.
- Grinsted, A.: An estimate of global glacier volume, The Cryosphere, 7, 141–151, https://doi.org/10.5194/tc-7-141-2013, 2013.
- Gupta, H., Wagener, T., and Liu, Y.: Reconciling Theory with Observations: Elements of a Diagnostic Approach to Model Evaluation, Hydrological Processes, 22, 3802–3813, https://doi.org/10.1002/hyp.6989, 2008.
- Hao, X., Huang, G., Zheng, Z., Sun, X., Ji, W., Zhao, H., Wang, J., Li, H., and Wang, X.: Development and validation of a new MODIS snow-cover-extent product over China, Hydrol. Earth Syst. Sci., 26, 1937–1952, https://doi.org/10.5194/hess-26-1937-2022, 2022.
- He, Y.: Pan-TPE soil map based on Harmonized World Soil Database (V1.2), National Tibetan Plateau Data Center, https://data.tpdc.ac.cn/zh-hans/data/3519536a-d1e7-4ba1-8481-6a0b56637baf/?q=HWSD (last access: 1 January 2019), 2019.
- He, Z., Vorogushyn, S., Unger-Shayesteh, K., Gafurov, A., Kalashnikova, O., Omorova, E., and Merz, B.: The Value of Hydrograph Partitioning Curves for Calibrating Hydrological Models in Glacierized Basins, Water Resources Research, 54, 2336–2361, https://doi.org/10.1002/2017WR021966, 2018.
- He, Z., Unger-Shayesteh, K., Vorogushyn, S., Weise, S. M., Kalashnikova, O., Gafurov, A., Duethmann, D., Barandun, M., and Merz, B.: Constraining hydrological model parameters using water isotopic compositions in a glacierized basin, Central Asia, Journal of Hydrology, 571, 332–348, https://doi.org/10.1016/j.jhydrol.2019.01.048, 2019.
- He, Z., Duethmann, D., and Tian, F.: A meta-analysis based review of quantifying the contributions of runoff components to streamflow in glacierized basins, Journal of Hydrology, 603, 126890, https://doi.org/10.1016/j.jhydrol.2021.126890, 2021.
- Hindshaw, R. S., Tipper, E. T., Reynolds, B. C., Lemarchand, E., Wiederhold, J. G., Magnusson, J., Bernasconi, S. M., Kretzschmar, R., and Bourdon, B.: Hydrological control of stream water chemistry in a glacial catchment (Damma Glacier, Switzerland), Chemical Geology, 285, 215–230, https://doi.org/10.1016/j.chemgeo.2011.04.012, 2011.

- Hugonnet, R., McNabb, R., Berthier, E., Menounos, B., Nuth, C., Girod, L., Farinotti, D., Huss, M., Dussaillant, I., Brun, F., and Kaab, A.: Accelerated global glacier mass loss in the early twenty-first century, Nature, 592, 726–731, https://doi.org/10.1038/s41586-021-03436-z, 2021.
- Huss, M. and Hock, R.: A new model for global glacier change and sea-level rise, Frontiers in Earth Science, 3, https://doi.org/10.3389/feart.2015.00054, 2015.
- Jasechko, S.: Global Isotope Hydrogeology–Review, Reviews of Geophysics, 57, 835–965, https://doi.org/10.1029/2018RG000627, 2019.
- Jasechko, S. and Taylor, R.: Intensive rainfall recharges tropical groundwaters, Environmental Research Letters, 10, 124015, https://doi.org/10.1088/1748-9326/10/12/124015, 2015.
- Jiang, Y., Yang, K., Yang, H., Lu, H., Chen, Y., Zhou, X., Sun, J., Yang, Y., and Wang, Y.: Characterizing basin-scale precipitation gradients in the Third Pole region using a high-resolution atmospheric simulation-based dataset, Hydrol. Earth Syst. Sci., 26, 4587–4601, https://doi.org/10.5194/hess-26-4587-2022, 2022.
- Jin, X., Xu, C. Y., Zhang, Q., and Singh, V.: Parameter and modeling uncertainty simulated by GLUE and a formal Bayesian method for a conceptual hydrological model, Journal of Hydrology, 383, 147–155, https://doi.org/10.1016/j.jhydrol.2009.12.028, 2010.
- Khakbaz, B., Imam, B., Hsu, K., and Sorooshian, S.: From lumped to distributed via semi-distributed: Calibration strategies for semi-distributed hydrologic models, Journal of Hydrology, 418–419, 61–77, https://doi.org/10.1016/j.jhydrol.2009.02.021, 2012.
- Khanal, S., Lutz, A. F., Kraaijenbrink, P. D. A., van den Hurk, B., Yao, T., and Immerzeel, W. W.: Variable 21st Century Climate Change Response for Rivers in High Mountain Asia at Seasonal to Decadal Time Scales, Water Resources Research, 57, https://doi.org/10.1029/2020wr029266, 2021.
- Lamontagne, J. and Barber, C.: Improved Estimators of Model Performance Efficiency for Skewed Hydrologic Data, Water Resources Research, 56, https://doi.org/10.1029/2020WR027101, 2020.
- Lin, J., Bryan, B. A., Zhou, X., Lin, P., Do, H. X., Gao, L., Gu, X., Liu, Z., Wan, L., Tong, S., Huang, J., Wang, Q., Zhang, Y., Gao, H., Yin, J., Chen, Z., Duan, W., Xie, Z., Cui, T., Liu, J., Li, M., Li, X., Xu, Z., Guo, F., Shu, L., Li, B., Zhang, J., Zhang, P., Fan, B., Wang, Y., Zhang, Y., Huang, J., Li, X., Cai, Y., and Yang, Z.: Making China's water data accessible, usable and shareable, Nature Water, 1, 328–335, https://doi.org/10.1038/s44221-023-00039-y, 2023.
- Liu, S.: The second glacier inventory dataset of China (version 1.0) (2006–2011), National Tibetan Plateau Data Center [data set], https://doi.org/10.3972/glacier.001.2013.db, 2012.
- Lutz, A. F., Immerzeel, W. W., Shrestha, A. B., and Bierkens, M. F. P.: Consistent increase in High Asia's runoff due to increasing glacier melt and precipitation, Nature Climate Change, 4, 587–592, https://doi.org/10.1038/nclimate2237, 2014.
- Lutz, A. F., Immerzeel, W. W., Kraaijenbrink, P. D. A., Shrestha, A. B., and Bierkens, M. F. P.: Climate Change Impacts on the Upper Indus Hydrology: Sources, Shifts and Extremes, Plos One, 11, https://doi.org/10.1371/journal.pone.0165630, 2016.
- Ma, J., Li, R., Zheng, H., Li, W., Rao, K., Yang, Y., and Wu,B.: Multivariate adaptive regression splines-assisted approximate Bayesian computation for calibration of complex hy-

- drological models, Journal of Hydroinformatics, 26, 503–518, https://doi.org/10.2166/hydro.2024.232, 2024.
- Majone, B., Avesani, D., Zulian, P., Fiori, A., and Bellin, A.: Analysis of high streamflow extremes in climate change studies: how do we calibrate hydrological models?, Hydrol. Earth Syst. Sci., 26, 3863–3883, https://doi.org/10.5194/hess-26-3863-2022, 2022.
- McGuire, K. J. and McDonnell, J. J.: A review and evaluation of catchment transit time modeling, Journal of Hydrology, 330, 543–563, 2006.
- McKay, M. D., Beckman, R. J., and Conover, W. J.: A Comparison of Three Methods for Selecting Values of Input Variables in the Analysis of Output from a Computer Code, Technometrics, 21, 239–245, 1979.
- Mohammadi, B., Gao, H., Feng, Z., Pilesjö, P., Cheraghalizadeh, M., and Duan, Z.: Simulating Glacier Mass Balance and its Contribution to Runoff in Northern Sweden, Journal of Hydrology, 620, https://doi.org/10.1016/j.jhydrol.2023.129404, 2023.
- Molotch, N. P. and Margulis, S. A.: Estimating the distribution of snow water equivalent using remotely sensed snow cover data and a spatially distributed snowmelt model: A multi-resolution, multi-sensor comparison, Advances in Water Resources, 31, 1503–1514, https://doi.org/10.1016/j.advwatres.2008.07.017, 2008.
- Moriasi, D., Arnold, J., Van Liew, M., Bingner, R., Harmel, R., and Veith, T.: Model Evaluation Guidelines for Systematic Quantification of Accuracy in Watershed Simulations, Transactions of the ASABE, 50, https://doi.org/10.13031/2013.23153, 2007.
- Muñoz-Sabater, J., Dutra, E., Agustí-Panareda, A., Albergel, C., Arduini, G., Balsamo, G., Boussetta, S., Choulga, M., Harrigan, S., Hersbach, H., Martens, B., Miralles, D. G., Piles, M., Rodríguez-Fernández, N. J., Zsoter, E., Buontempo, C., and Thépaut, J.-N.: ERA5-Land: a state-of-the-art global reanalysis dataset for land applications, Earth Syst. Sci. Data, 13, 4349–4383, https://doi.org/10.5194/essd-13-4349-2021, 2021.
- Myneni, R., Knyazikhin, Y., and Park, T.: MOD15A2H MOD-IS/Terra Leaf Area Index/FPAR 8-Day L4 Global 500 m SIN Grid V006 NASA EOSDIS Land Processes DAAC [data set], https://doi.org/10.5067/MODIS/MOD15A2H.006, 2015.
- Nan, Y. and Tian, F.: Isotope data-constrained hydrological model improves soil moisture simulation and runoff source apportionment, Journal of Hydrology, 633, 131006, https://doi.org/10.1016/j.jhydrol.2024.131006, 2024.
- Nan, Y., He, Z., Tian, F., Wei, Z., and Tian, L.: Can we use precipitation isotope outputs of isotopic general circulation models to improve hydrological modeling in large mountainous catchments on the Tibetan Plateau?, Hydrol. Earth Syst. Sci., 25, 6151–6172, https://doi.org/10.5194/hess-25-6151-2021, 2021a.
- Nan, Y., Tian, L., He, Z., Tian, F., and Shao, L.: The value of water isotope data on improving process understanding in a glacierized catchment on the Tibetan Plateau, Hydrol. Earth Syst. Sci., 25, 3653–3673, https://doi.org/10.5194/hess-25-3653-2021, 2021b.
- Nan, Y., He, Z., Tian, F., Wei, Z., and Tian, L.: Assessing the influence of water sampling strategy on the performance of tracer-aided hydrological modeling in a mountainous basin on the Tibetan Plateau, Hydrol. Earth Syst. Sci., 26, 4147–4167, https://doi.org/10.5194/hess-26-4147-2022, 2022.
- Nan, Y., Tian, F., Li, Z., and Gui, J.: Longer simulation time step of the tracer-aided hydrological model estimates lower contribu-

- tion of slow runoff components, Journal of Hydrology, 129889–129889, https://doi.org/10.1016/j.jhydrol.2023.129889, 2023.
- Nan, Y., Tian, F., and Li, Z.: Model Diagnostic Analysis in a Cold Basin Influenced by Frozen Soils With the Aid of Stable Isotope, Water Resources Research, 60, https://doi.org/10.1029/2024WR037218, 2024.
- Nan, Y. and Avesani, D.: Model output for "Reducing Hydrological Uncertainty in Large Mountainous Basins: The Role of Isotope, Snow Cover, and Glacier Dynamics in Capturing Streamflow Seasonality", Zenodo [data set], https://doi.org/10.5281/zenodo.15605202, 2025a.
- Nan, Y. and Avesani, D.: Dataset for "Reducing Hydrological Uncertainty in Large Mountainous Basins: The Role of Isotope, Snow Cover, and Glacier Dynamics in Capturing Streamflow Seasonality", Zenodo [data set], https://doi.org/10.5281/zenodo.16634369, 2025b.
- Nan, Y., Tian, F., McDonnell, J., Ni, G., Tian, L., Li, Z., Yan, D., Xia, X., Wang, T., Han, S., and Li, K.: Glacier meltwater has limited contributions to the total runoff in the major rivers draining the Tibetan Plateau, Npj Climate and Atmospheric Science, 8, https://doi.org/10.1038/s41612-025-01060-6, 2025.
- Nash, J. and Sutcliffe, J.: River flow forecasting through conceptual models part I – A discussion of principles, Journal of Hydrology, 10, 282–290, https://doi.org/10.1016/0022-1694(70)90255-6, 1970.
- O'Neel, S., Hood, E., Arendt, A., and Sass, L.: Assessing streamflow sensitivity to variations in glacier mass balance, Climatic Change, 123, 329–341, https://doi.org/10.1007/s10584-013-1042-7, 2014.
- Panchanathan, A., Ahrari, A., Ghag, K. S., Mustafa, S., Haghighi, A. T., Kløve, B., and Oussalah, M.: An overview of approaches for reducing uncertainties in hydrological forecasting: Progress and challenges, Earth-Science Reviews, 258, 104956, https://doi.org/10.1016/j.earscirev.2024.104956, 2024.
- Raleigh, M. S., Lundquist, J. D., and Clark, M. P.: Exploring the impact of forcing error characteristics on physically based snow simulations within a global sensitivity analysis framework, Hydrol. Earth Syst. Sci., 19, 3153–3179, https://doi.org/10.5194/hess-19-3153-2015, 2015.
- Reggiani, P., Hassanizadeh, S., Sivapalan, M., and Gray, W. G.: A unifying framework for watershed thermodynamics: constitutive relationships, Advances in Water Resources, 23, 15–39, https://doi.org/10.1016/S0309-1708(99)00005-6, 1999.
- Rodgers, P., Soulsby, C., Waldron, S., and Tetzlaff, D.: Using stable isotope tracers to assess hydrological flow paths, residence times and landscape influences in a nested mesoscale catchment, Hydrol. Earth Syst. Sci., 9, 139–155, https://doi.org/10.5194/hess-9-139-2005, 2005.
- Ruelland, D.: Potential of snow data to improve the consistency and robustness of a semi-distributed hydrological model using the SAFRAN input dataset, Journal of Hydrology, 631, 130820, https://doi.org/10.1016/j.jhydrol.2024.130820, 2024.
- Shuai, P., Chen, X., Mital, U., Coon, E. T., and Dwivedi, D.: The effects of spatial and temporal resolution of gridded meteorological forcing on watershed hydrological responses, Hydrol. Earth Syst. Sci., 26, 2245–2276, https://doi.org/10.5194/hess-26-2245-2022, 2022.
- Stahl, K., Moore, R. D., Shea, J. M., Hutchinson, D., and Cannon, A. J.: Coupled modelling of glacier and streamflow re-

- sponse to future climate scenarios, Water Resources Research, 44, https://doi.org/10.1029/2007WR005956, 2008.
- Sun, H., Yao, T., Su, F., Yang, W., and Chen, D.: Spatiotemporal responses of runoff to climate change in the southern Tibetan Plateau, Hydrol. Earth Syst. Sci., 28, 4361–4381, https://doi.org/10.5194/hess-28-4361-2024, 2024.
- Tetzlaff, D., Birkel, C., Dick, J., and Geris, J.: Storage dynamics in hydropedological units control hillslope connectivity, runoff generation, and the evolution of catchment transit time distributions, Water Resources Research, 50, 969–985, https://doi.org/10.1002/2013WR014147, 2014.
- Teweldebrhan, A. T., Burkhart, J. F., and Schuler, T. V.: Parameter uncertainty analysis for an operational hydrological model using residual-based and limits of acceptability approaches, Hydrol. Earth Syst. Sci., 22, 5021–5039, https://doi.org/10.5194/hess-22-5021-2018, 2018.
- Tian, F., Hu, H., Lei, Z., and Sivapalan, M.: Extension of the Representative Elementary Watershed approach for cold regions via explicit treatment of energy related processes, Hydrol. Earth Syst. Sci., 10, 619–644, https://doi.org/10.5194/hess-10-619-2006, 2006.
- Tong, R., Parajka, J., Salentinig, A., Pfeil, I., Komma, J., Széles, B., Kubáň, M., Valent, P., Vreugdenhil, M., Wagner, W., and Blöschl, G.: The value of ASCAT soil moisture and MODIS snow cover data for calibrating a conceptual hydrologic model, Hydrol. Earth Syst. Sci., 25, 1389–1410, https://doi.org/10.5194/hess-25-1389-2021, 2021.
- Tong, R., Parajka, J., Széles, B., Greimeister-Pfeil, I., Vreugdenhil, M., Komma, J., Valent, P., and Blöschl, G.: The value of satellite soil moisture and snow cover data for the transfer of hydrological model parameters to ungauged sites, Hydrol. Earth Syst. Sci., 26, 1779–1799, https://doi.org/10.5194/hess-26-1779-2022, 2022.
- Vrugt, J. A. and Sadegh, M.: Toward diagnostic model calibration and evaluation: Approximate Bayesian computation, Water Resources Research, 49, 4335–4345, https://doi.org/10.1002/wrcr.20354, 2013.
- Wu, Y., Sun, J., Blanchette, M., Rousseau, A. N., Xu, Y. J., Hu, B., and Zhang, G.: Wetland mitigation functions on hydrological droughts: From drought characteristics to propagation of meteorological droughts to hydrological droughts, Journal of Hydrology, 617, 128971, https://doi.org/10.1016/j.jhydrol.2022.128971, 2023.
- Xu, M., Yan, M., Kang, J., and Ren, J.: Comparative studies of glacier mass balance and their climatic implications in Svalbard, Northern Scandinavia, and Southern Norway, Environmental Earth Sciences, 67, 1407–1414, https://doi.org/10.1007/s12665-012-1585-3, 2012.
- Xu, R., Tian, F., Yang, L., Hu, H., Lu, H., and Hou, A.: Ground validation of GPM IMERG and TRMM 3B42V7 rainfall products over southern Tibetan Plateau based on a high-density rain gauge network, Journal of Geophysical Research: Atmospheres, 122, 910–924, https://doi.org/10.1002/2016JD025418, 2017.
- Yang, J., Reichert, P., and Abbaspour, K. C.: Bayesian uncertainty analysis in distributed hydrologic modeling: A case study in the Thur River basin (Switzerland), Water Resources Research, 43, https://doi.org/10.1029/2006WR005497, 2007.
- Yang, K. and He, J.: China meteorological forcing dataset (1979–2018), National Tibetan Plateau Data Center,

- https://doi.org/10.11888/AtmosphericPhysics.tpe.249369.file, 2019.
- Yang, L., Feng, Q., Ning, T., Lu, T., Zhu, M., Yin, X., and Wang, J.: Attributing the streamflow variation by incorporating glacier mass balance and frozen ground into the Budyko framework in alpine rivers, Journal of Hydrology, 628, 130438, https://doi.org/10.1016/j.jhydrol.2023.130438, 2024.
- Yapo, P. O., Gupta, H. V., and Sorooshian, S.: Multi-objective global optimization for hydrologic models, Journal of Hydrology, 204, 83–97, https://doi.org/10.1016/S0022-1694(97)00107-8, 1998.
- Yoshimura, K., Kanamitsu, M., Noone, D., and Oki, T.: Historical isotope simulation using Reanalysis atmospheric data, Journal of Geophysical Research-Atmospheres, 113, https://doi.org/10.1029/2008jd010074, 2008.
- Zhang, M., Nan, Y., and Tian, F.: Runoff component quantification and future streamflow projection in a large mountainous basin based on a multidata-constrained cryospherichydrological model, Hydrol. Earth Syst. Sci., 29, 1033–1060, https://doi.org/10.5194/hess-29-1033-2025, 2025.
- Zhang, Q., Knowles, J. F., Barnes, R. T., Cowie, R. M., Rock, N., and Williams, M. W.: Surface and subsurface water contributions to streamflow from a mesoscale watershed in complex mountain terrain, Hydrological Processes, 32, 954–967, https://doi.org/10.1002/hyp.11469, 2018.